SCMS SCHOOL OF ENGINEERING & TECHNOLOGY

BOOK/CONFERENCE DETAILS 2020

Sl No:	Name	First Author	Second Author	Third Author	Fourth Author	INDEXING
1	Dr.Sreeja K A	CEC2001,CEC2002				conference-BOOK PROCEEDI
2	Dr.Sunil Jacob	CEC2003				conference-BOOK PROCEEDI
3	Dr.Nuja Unnikrishnan	CBSH2001				conference
4	Jane Theresa	BBSH2002				book chapters
5	Remya Y K	CCE2001				conference
6	Sruthy M R	CCE2002	CCE2003			conference
7	Dr.Akhila M	CCE2003,BCE2001	CCE2002			conference
8	Anjana Susan John	CCE2004				conference
9	Dr.Sreeja Rajesh	CCSE2006				conference
10	Dr. Varun G Menon		CEC2003		CCSE2001	conference-BOOK PROCEEDINGS
11	Litty Koshy	CCSE2002	CCSE2005			conference-BOOK PROCEEDINGS
12	Neenu Sebastian			CCSE2004		conference-BOOK PROCEEDINGS
Total Book/Conference for the calender year 2020						**15**

DR. PRAVEENSAL C.J.
PRINCIPAL
SCMS SCHOOL OF ENGINEERING & TECHNOLOGY

Retinal Image Enhancement by Intensity Index Based Histogram Equalization for Diabetic Retinopathy Screening

Arun Pradeep, X. Felix Joseph, and K. A. Sreeja

1 Introduction

Retinal exudates that can be visually identified as yellow flecks in fundus images and is considered one of the symptoms arised due to Diabetic Retinopathy. These are mainly due to leakage of lipids in the eyes from the damaged capillaries as shown in Fig. 1. Diagnosis done at an earlier stage can control the degree of impairment caused by leakage of lipids that can ultimately lead to loss of eyesight. Patient friendly studies are centered on the accuracy of exudate detection from RGB fundus images with the help of machine learning.

These images are captured using a fundus camera which may contain effects of noise and uneven illumination and contrast. In order to filter out these undesired effects, literature suggests that pre-processing and image enhancement should be more focused before image segmentation and classification. The study presented by [1] identifies retinal exudates established on spider monkey optimization using an SMO-GBM classifier. Likewise, the image enhancement was done using contourlet transform. The method proposed in [2] uses classification based on Top-k loss method instead of Class Balance Entropy (CBCE) to reduce misclassification in exudate detection.

A. Pradeep (✉)
Noorul Islam University, Thucklay, Kanyakumari, India

X. F. Joseph
Bule Hora University, Hagere Maryam, Ethiopia

K. A. Sreeja
SCMS School of Engineering and Technology, Ernakulam, India

A. Haldorai et al. (eds.), *2nd EAI International Conference on Big Data Innovation for Sustainable Cognitive Computing*, EAI/Springer Innovations in Communication and Computing, https://doi.org/10.1007/978-3-030-47560-4_8

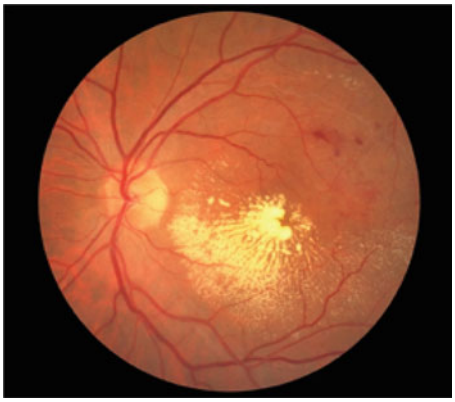

Fig. 1 Fundus image of diabetic eye

The analysis in [3] proposes that Convolutional Neural Network (CNN) can be utilized for a deep learning technique, for exudate detection, but the efficiency is deprived when compared with Residual Network and Discriminative Restricted Boltzmann machines. The color space used in our work is HSI instead of RGB, which gives more attenuation to noise. This method is reiterated by the work suggested by Khojasteh et al. [4] for exudate detection. Holistic texture features of fundus images were extracted and trained to four different classifiers in the study [5] conducted on a public database. Classification of hard exudates from soft exudate using fuzzy logic was the area of interest in [6]. Segmentation of exudates using dynamic decision thresholding was the focus of study in [7]. Their results were validated using lesion and image based evaluation criteria. Circular Hough Transform(CHT) and CNN based detection of exudates were suggested in [8]. A reduced pre-processing strategy for exudate based macular edema recognition using deep residual network was put forward in [9]. Multilayer perceptron based supervised learning is studied in [10] to identify exudate pixels. Further segmentation was done using unsupervised learning with the help of iterative Graph Cut (GC). The entire image is segmented into a series of super pixels in [11] which are considered as candidate pixels.

Also each candidate is characterized by multi-channel intensity features and contextual features. The study in [12] using a neighborhood estimator presents detection of blood vessels followed by segmentation with the help of in-painting the exudates with the help of this estimator. A new approach called voxel classification by a strategy based on layer dependent stratified sampling on OCT image was introduced in [13]. Grayscale morphology based segmentation of exudates was presented in [14] where the candidate pixels' shape was determined with the help of Markovian Segmentation model. Another method using Partial Least Squares (PLS) for detection of exudates is studied in [15]. An image segmentation based high level entity known as splat is used to identify retinal hemorrhages in [16] where pixels sharing similar properties are grouped together to form non-overlapping splats and the features are extracted and classified using supervised learning. The research

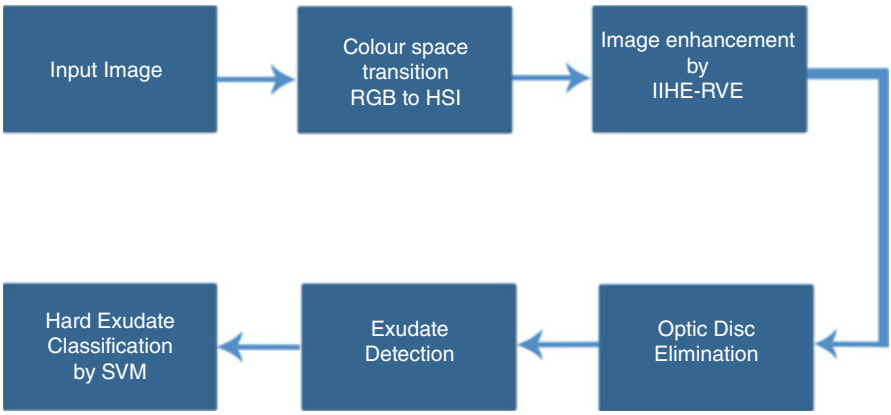

Fig. 2 Depiction of total work flow

study presented in this paper is a modification of our existing algorithm presented in [17]. The method associates both the principles of mathematical morphology operation for detection of exudates and classification and extraction of exudates using a trained classifier. Before the mathematical binary operation, initial pre-processing is done to enhance the fundus image where an algorithm called Intensity Index based Histogram Equalization Technique for retinal vessel enhancement (IIHE-RVE) is proposed. The algorithm of the total work is depicted in Fig. 2.

2 Methodology

Color plane transition from RGB to HSI is performed because the Optic Disc (OD) as well as exudates have analogous brightness characteristics. Many of the imperfections caused by noise and texture in the image can also be reduced by transition to HSI plane [18]. Median filter is applied to reduce the noise in the intensity band of the image. A novel method called Intensity Index based Histogram Equalization Technique for retinal vessel enhancement (IIHE-RVE) is applied to enhance the contrast of the noise free image.

IIHE-RVE is based on the estimation of under radiance of the image which is more effective than the existing Contrast limited adaptive Histogram equalization (CLAHE) algorithm or any other Gaussian function equalization algorithms. The following step is involved in the removal of Optic Disc (OD). It is assumed that the OD exist as the largest bright circular shape component in the image. Finally, exudates are classified into hard and soft exudates using a supervised classifier. Clinical images as well as images from publically available database are validated for the proposed algorithm.

2.1 Image Enhancement

The pre-processing steps involved in this work are shown in Fig. 3. RGB to HSI transition is followed by median filtering and contrast enhancement is done the new technique of histogram equalization.

Applying a tunable parameter ξ, histograms are divided into sub-histograms by computing the split value using the following set of Eqs. 1 and 2

$$\alpha_c(i) = \frac{\phi(i)}{\epsilon} \quad \text{for} \quad 0 \leq i \leq I - 1 \tag{1}$$

$$\Gamma(k) = \sum_{i=0}^{k} \alpha_c(i) \quad \text{for} \quad 0 \leq k \leq I - 1 \tag{2}$$

where ϕ denotes the histogram of the image, i represents the intensity value, ϵ represents the pixel numbers for the whole image, and I signifies the total brightness levels in numbers. The parameters Γ and α_c give accumulated normalized histogram count and normalized histogram count, respectively, for the given image. The controlling parameter Γ_p is found by Eq. 3.

$$\sum_{j=0}^{\Gamma_p} \Gamma(j) \approx \xi \quad \text{for any } 0.1 \leq \xi \leq 0.9 \tag{3}$$

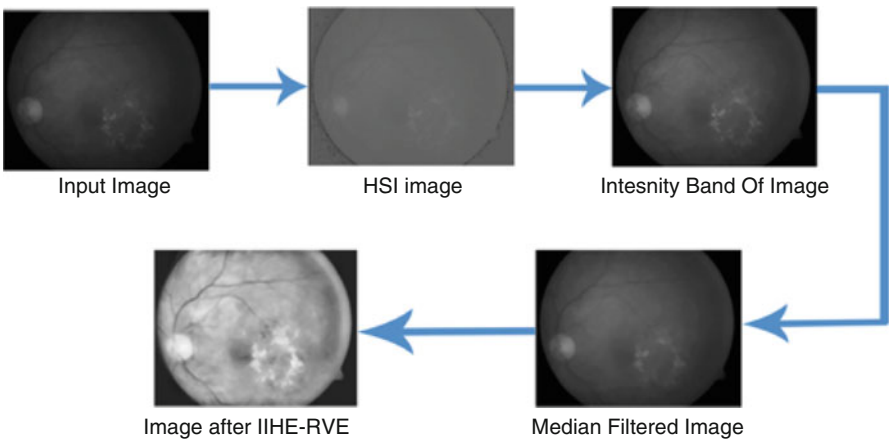

Fig. 3 Steps involved in pre-processing

The split value S_v is found from Eq. 4.

$$S_v = (I - 1) - \Gamma_p - 1 \tag{4}$$

The value of tunable parameter ξ is inversely proportional to enhancement level of the image. Also when ξ increases the value of Γ_p also increases. For a certain low value of ξ, we can acquire a first sub-histogram and for another high value of ξ we can acquire a second sub-histogram. The first and second sub-histograms are equalized specifically. Due to the extendedness of these histograms, the range of pixels having lower intensity can be mapped to a range of higher intensity. Whereas, in the second sub-histogram, the range is less and contains only larger intensity range pixels. Because of this small range, the larger intensity pixels are saved from over enhancement.

2.2 *Intensity Index Based Histogram Equalization Technique for Retinal Vessel Enhancement (IIHE-RVE)*

According to the algorithm, when the two histograms are obtained, successive integration based on difference of intensity parameters obtained from the iteratively enhanced images is performed. Integration is continued till the absolute difference between the intensity values ω_1 and ω_2 obtained from Eq. 5, for the given image and the equalized image is lower than error referred to as threshold, e. Here, the value of e is taken as 0.002.

Algorithm 1 IIHE algorithm

1: Compute histogram ϕ for image f.
2: Compute intensity values for input image from Eq. 5 for $I = 256$.

$$\omega_1 = \frac{\sum_{i=0}^{I-1} \phi(i) \cdot i}{I \cdot \sum_{i=0}^{I-1} \phi(i)} \tag{5}$$

3: S_v which is the split value is calculated from Eq. 4.
4: Separate the histogram into sub-histograms ϕ_l from radiance range 0 to S_v and ϕ_u from S_{v+1} to $I - 1$.
5: Equalize histograms ϕ_l and ϕ_u in the respective intensity range.
6: Reiterate Step 2 to find the intensity values ω_2 of equalized image.
7: Repeat steps 1–6 until $|\omega_1 - \omega_2| \leq e$.
8: Integrate ϕ_l and ϕ_u to re-establish histogram ϕ.

2.3 Optic Disc Elimination

The exudates have similar intensity values as that of optic disc. Opening and Closing are the two binary operations used for detection of OD in retinal image. The shape of the OD is obtained from the image I by employing the mathematical closing operation. Using a threshold operation, the suitable binary image is produced.

The binary image Ω contains various connected components known as C_i which is based on Eq. 6.

$$\Omega = \bigcup_{k \in m} C_k, C_i \bigcap C_j = 0, \quad \forall \quad i, j \in m, \quad i \neq j \tag{6}$$

where m varies from 1 to k, k symbolizes the connected components. The disc shape structure when compared to the background pixels are the components of C_i. This includes the OD also. Hence, an effective separation of OD from other structures is established. Now, R_i becomes the greatest component that is connected in C_i . The conciseness of R_i is calculated using Eq. 7:

$$C(R_i) = 4\pi \frac{A(R_i)}{P^2(R_i)} \tag{7}$$

In this equation, $A(R_i)$ signifies pixels' number in the ith region and $P(R_i)$ represents the pixels in region (R_i). Another threshold method is obtained from P-tile method [19] and Nilback's method[20, 21] in order to obtain the binary image.

The weight factor chosen is 1.3 based on previous conclusions in our method [17]. In order to delineate the OD on the retinal image, Circular Hough Transformation (CHT) is employed as studied in[22]. The OD elimination is depicted in Fig. 4.

2.4 Detection of Exudates

After optic disc elimination, exudate pixels are identified. Using binary closing operation a 16-pixel radius, flat disc shaped structuring element is utilized and the exudates pixels are directly identified. Binary closing operation follows this threshold operation. The blood vessels have a contrast component which is similar to the contrast component applied in this operation. Hence the image's Standard Deviation (SD) is calculated using Eq. 8.

$$I_3(x) = \frac{1}{N-1} \sum_{i \in W(x)} \left(I_2(i) - \overline{I_3(x)}\right)^2 \tag{8}$$

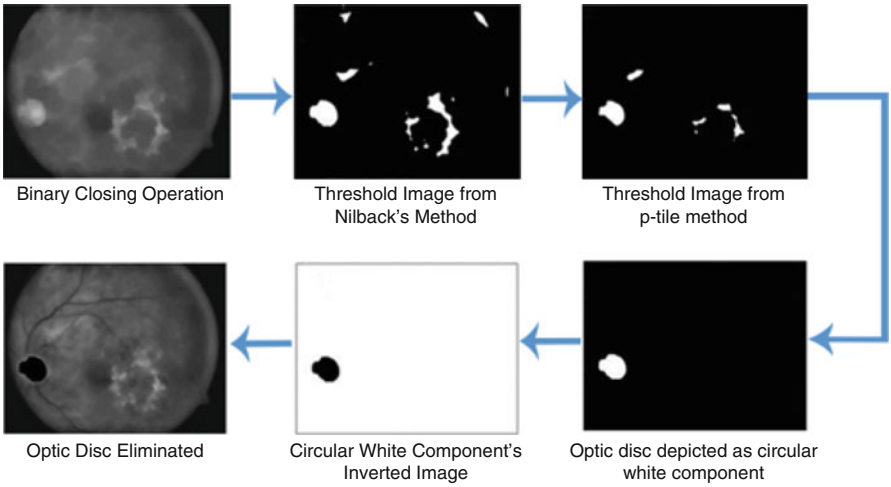

Fig. 4 Steps involved in OD elimination

In this above equation, $W(x)$ symbolizes available pixels available for a sub-window, N symbolizes pixels available in $W(x)$ and $\overline{I_3(x)}$ give the average value for the image $I_3(x)$ where the local contrast image is symbolized by I_3. Using a method called Triangle based threshold [23], the bright regions can be precisely detected and the components can be differentiated. Followed by identification of the high intensity regions, unwanted pixels on the image are eliminated using binary operation called dilation. This method is followed by a flood fill operation that is done on holes so as to regenerate the image. Next, the final step involved in exudate detection is difference image acquisition between from the output image from the threshold image, which is nothing but the brightness based image. As a result, the difference image is superimposed on the original image in order to extract exudate features from the pixels. The whole process of detection of exudates is illustrated in Fig. 5.

2.5 Hard Exudate Classification

The final operation which is the classification of hard exudates from the exudate pixels comprises of a valuation using the features that are usually employed by ophthalmologists to visually distinguish hard exudates. The same features are employed as SVM Classifier's input. The set of features is mentioned in Table 1.

Compared with features published in algorithms [24–26], the above eight features were measured important to decrease processing time by not compromising the efficiency for hard exudate classification. The features mentioned in Table 1 are given to the input of an SVM classifier where the output shows the classification

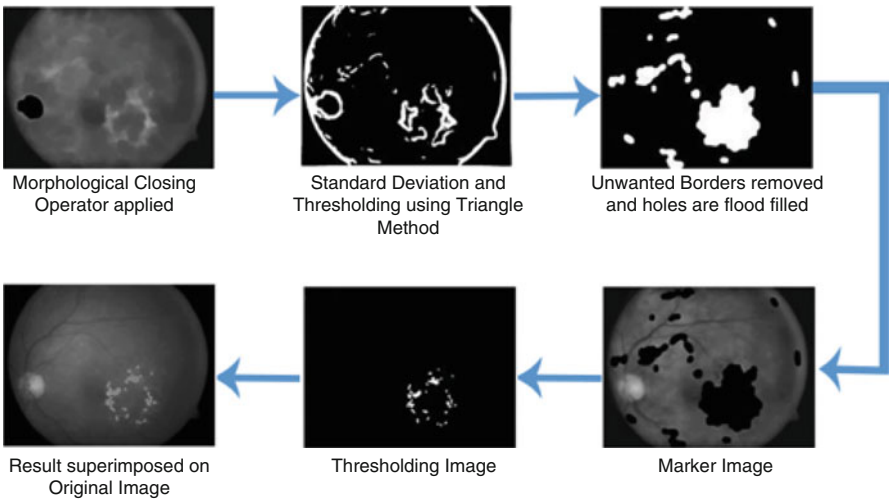

Fig. 5 Steps involved in exudate detection

Table 1 Feature sets for hard exudate classification

Feature sl. no.	Feature type	Description
f_1	Green intensity of mean channel	The green channel image is applied with a 3×3 size Mean filter in order to find each pixels's gray scale intensity
f_2	Gray intensity	Pixel's gray scale value
f_3 f_4 f_5	Mean saturation, mean hue and mean intensity of HSI color model	A 3×3 size Mean filter is respectively applied to the images I_h, I_s, I_i. Now, f_4 and f_5 refers to saturation and brightness as exudates can be seen as bright lesions
f_6	Energy	Intensity square of pixels and its summation
f_7	Standard deviation	SD is performed and the foreground regions are preserved in the image which have characteristics similar to structuring element
f_8	Mean gradient magnitude	The edge pixels' intensity in terms of directional change in magnitude

results in the form of a binary matrix. SVM is applied over Radial Basis Function (RBF) kernel. The evaluation using cross validation was performed using the gold standard images obtained from Dr. Bejan Singh Eye Hospital and selected by an expert. A total of 72 images were selected from the gold standard for training. The pixels were categorized as non-exudate regions and exudate regions. The cross validation was performed in ten folds to check the SVM classifier's efficiency.

The database images from DIARETDB1 were selected and split arbitrarily into ten subsets (ten folds) which were mutually exclusive and has exudate connected

components. They are $B_1, B_2, B_3 \ldots B_{10}$ that have same size. Sixty-seven images were trained on the classifier from the gold standard and the remaining 5 were employed for testing. The output obtained was a binary matrix. And for cross validation the process was repeated ten times with each subset. Thus every pixel provided a vector set containing all the features mentioned in Table 1 as:

$$a_i = (f_1, f_2, f_3 \ldots f_8) \tag{9}$$

Another entity b_j is defined as a flag to define the category which is represented as

$$b_j = \begin{cases} -1 & a_i \in A \\ +1 & a_i \in B \end{cases} \tag{10}$$

where $j \subset \{1, 2, 3 \ldots W\}$ denotes the dimensions of the vector set sample. The hard exudate region is represented by A and the non-hard exudate region is represented by B.

The SVM classifier was trained using the sample set (a_i, b_j). The value of W is chosen as 4200, which means 4200 pixels in 67 samples were categorized by the expert.

2.6 Evaluation Parameters

In this research work, the database candidate subset is considered as $\{B_1, B_2, B_3, \ldots B_N\}$ and gold standard subset is $\{T_1, T_2, T_3, \ldots T_M\}$.

The equation for a pixel to be True Positive (TP) is given in Eq. 11

$$\{B \cap T\} \cup \left\{ B_i | \frac{|B_i \cap T|}{B_i} > \sigma \right\} \cup \left\{ T_j | \frac{|T_j \cap B|}{T_j} > \sigma \right\} \tag{11}$$

In this research work the σ value is fixed at 0.2 which has a global range of {0,1}. The equation for a pixel to be False Positive (FP) is given in Eq. 12.

$$\{B_i | B_i \cap T = \phi\} \cup \left\{ B_i \cap \overline{T} | \frac{|B_i \cap T|}{|B_i|} \leq \sigma \right\} \tag{12}$$

The equation for a pixel to be False Negative (FN) is given in Eq. 13

$$\{T_j | T_j \cap B = \phi\} \cup \left\{ T_j \cap \overline{B} | \frac{|T_j \cap B|}{|T_j|} \leq \sigma \right\} \tag{13}$$

Finally, all the remaining pixels can be referred to True Negatives (TN).

3 Results and Discussions

There are mainly two sources for the fundus image acquisition. Dr. Bejan Singh Eye Hospital provided with the clinical image which were captured by "Remidio Non-Mydriatic Fundus On Phone (FOP-NM10)" [27] Fundus camera having a Field-Of-View: 40°, having 100–400 ISO range and has a 33 mm working distance. The public database DIARETDB1 was utilized for images required for validation. Table 2 shows the observations of 30 images that were validated.

Since there is an asymmetry between the classes of TP, FN, and FP when compared with TN, by computing just the Area Under Curve (AUC) of Receiver operator

Table 2 Performance matrix evaluated for 30 fundus images

	TP	FP	FN	TN	Accuracy	Sensitivity	Specificity	PPV	F-score
Image 1	349	78	35	431,651	99.97%	90.89%	99.98%	81.73%	86.07%
Image 2	372	106	35	431,487	99.97%	91.40%	99.98%	77.82%	84.07%
Image 3	6835	83	52	419,183	99.97%	99.24%	99.98%	98.80%	99.02%
Image 4	54	89	30	431,946	99.97%	64.29%	99.98%	37.76%	47.58%
Image 5	321	34	23	431,630	99.99%	93.31%	99.99%	90.42%	91.85%
Image 6	1488	31	80	429,122	99.97%	94.90%	99.99%	97.96%	96.40%
Image 7	409	26	37	431,420	99.99%	91.70%	99.99%	94.02%	92.85%
Image 8	964	40	54	430,947	99.98%	94.70%	99.99%	96.02%	95.35%
Image 9	6543	56	67	422,555	99.97%	98.99%	99.99%	99.15%	99.07%
Image 10	811	80	78	430,774	99.96%	91.23%	99.98%	91.02%	91.12%
Image 11	1166	49	52	430,535	99.98%	95.73%	99.99%	95.97%	95.85%
Image 12	3522	39	40	427,474	99.98%	98.88%	99.99%	98.90%	98.89%
Image 13	818	30	67	430,259	99.98%	92.43%	99.99%	96.46%	94.40%
Image 14	435	88	23	431,328	99.97%	94.98%	99.98%	83.17%	88.69%
Image 15	1536	40	57	428,684	99.98%	96.42%	99.99%	97.46%	96.94%
Image 16	623	56	35	431,002	99.98%	94.68%	99.99%	91.75%	93.19%
Image 17	3421	38	22	427,567	99.99%	99.36%	99.99%	98.90%	99.13%
Image 18	4090	49	25	427,468	99.98%	99.39%	99.99%	98.82%	99.10%
Image 19	233	39	55	431,731	99.98%	80.90%	99.99%	85.66%	83.21%
Image 20	785	30	22	431,053	99.99%	97.27%	99.99%	96.32%	96.79%
Image 21	327	88	15	431,563	99.98%	95.61%	99.98%	78.80%	86.39%
Image 22	1053	33	24	430,947	99.99%	97.77%	99.99%	96.96%	97.36%
Image 23	188	70	22	431,441	99.98%	89.52%	99.98%	72.87%	80.34%
Image 24	2213	44	21	429,216	99.98%	99.06%	99.99%	98.05%	98.55%
Image 25	964	33	37	430,750	99.98%	96.30%	99.99%	96.69%	96.50%
Image 26	521	25	6	431,650	99.99%	98.86%	99.99%	95.42%	97.11%
Image 27	848	90	5	429,132	99.98%	99.41%	99.98%	90.41%	94.70%
Image 28	904	24	56	431,480	99.98%	94.17%	99.99%	97.41%	95.76%
Image 29	842	99	34	430,927	99.97%	96.12%	99.98%	89.48%	92.68%
Image 30	4543	35	68	422,565	99.98%	98.53%	99.99%	99.24%	98.88%

characteristic (ROC) is not appropriate. So 5 different evaluation parameters are taken into consideration. They are

$$\text{accuracy} = \frac{\text{TN} + \text{TP}}{\text{TP} + \text{FP} + \text{TN} + \text{FN}} \tag{14}$$

$$\text{sensitivity} = \frac{\text{TP}}{\text{TP} + \text{FN}} \tag{15}$$

$$\text{specificity} = \frac{\text{TN}}{\text{TN} + \text{FP}} \tag{16}$$

$$\text{Positive Prediction Value (PPV)} = \frac{\text{TP}}{\text{TP} + \text{FP}} \tag{17}$$

$$F \text{ score} = 2 \times \frac{\text{sensitivity} \times \text{PPV}}{\text{sensitivity} + \text{PPV}} \tag{18}$$

The table shows good results with respect to the average sensitivity, specificity as well as accuracy having a value of 87%, 98%, and 98.7%, respectively. The F-score as well as the precision calculated were far higher than other works published in the literature in [28, 29] that is F-score = 89.91% and precision = 88.10%. Table 3 shows a comparative study with algorithms that were already published and it can be inferred that accuracy as well as specificity of this research work is greater than the other methods in literature.

Table 4 gives a comparison of the improved method of image enhancement that is IIHE-RVE with our previous method—contrast limited adaptive histogram equalization (CLAHE) which shows a reasonable increase in the value of specificity, PPV, and F-score.

Table 3 Comparison with existing algorithms

Methodology	Sensitivity	Specificity	Accuracy
Chen et al. [29]	83	75	79
Travieso et al. [30]	91.67	92.68	92.13
Barman et al. [31]	92.42	81.25	87.72
Proposed method	87.90	99.97	99.92
A Hajdu et al. [26]	92	68	82
R Sinha et al. [25]	96.54	93.15	N.A.
Pourreza et al. [28]	86.01	99.93	N.A.

Table 4 Performance matrix of 30 images evaluated

Methodology	Sensitivity	Specificity	Accuracy	PPV	F-score
CLAHE [17]	99.81%	80.06%	99.96%	88.03%	81.90%
IIHE-RVE	99.92%	87.90%	99.97%	89.91%	88.10%

4 Conclusion

The proposed work is a novel technique to detect exudates using morphological operation. The new enhancement method IIHE-RVE was used to increase the sensitivity of our existing algorithm that originally involved enhancement using CLAHE. A considerable increase in specificity indicates that the algorithm is more accurate while considering low intensity images. Using the same feature set to the classifier, the score of evaluation parameters could be increased by changing the enhancement technique. Further studies can be implicated to increase the PPV and F-score of this algorithm.

References

1. Badgujar RD, Deore PJ (2019) Hybrid nature inspired SMO-GBM classifier for exudate classification on fundus retinal images. Innov Res BioMed Eng 40(2):69–77
2. Guo S, Wang K, Kang H, Liu T, Gao Y, Li T (2019) Bin loss for hard exudates segmentation in fundus images. Neurocomputing 392:314–324
3. Khojasteh P et al (2019) Exudate detection in fundus images using deeply-learnable features. Comput Biol Med 104:62–69
4. Khojasteh P, Aliahmad B, Kumar DK (2019) A novel color space of fundus images for automatic exudates detection. Biomed Signal Process Control 49:240–249
5. Frazao LB, Theera-Umpon N, Auephanwiriyakul S (2019) Diagnosis of diabetic retinopathy based on holistic texture and local retinal features. Inf Sci (NY) 475:44–66
6. Kumar RS, Karthikamani R, Vinodhini S (2018) Mathematical morphology for recognition of hard exudates from diabetic retinopathy images. Int J Recent Technol Eng 7(4S):367–370
7. Kaur J, Mittal D (2018) A generalized method for the segmentation of exudates from pathological retinal fundus images. Biocybern Biomed Eng 38(1):27–53
8. Adem K (2018) Exudate detection for diabetic retinopathy with circular Hough transformation and convolutional neural networks. Expert Syst Appl 114:289–295
9. Mo J, Zhang L, Feng Y (2018) Exudate-based diabetic macular edema recognition in retinal images using cascaded deep residual networks. Neurocomputing 290:161–171
10. Kusakunniran W, Wu Q, Ritthipravat P, Zhang J (2018) Hard exudates segmentation based on learned initial seeds and iterative graph cut. Comput Methods Programs Biomed 158:173–183
11. Zhou W, Wu C, Yi Y, Du W (2017) Automatic detection of exudates in digital color fundus images using superpixel multi-feature classification. IEEE Access 5:17077–17088
12. Annunziata R, Garzelli A, Ballerini L, Mecocci A, Trucco E (2016) Leveraging multiscale Hessian-based enhancement with a novel exudate inpainting technique for retinal vessel segmentation. IEEE J Biomed Health Inform 20(4):1129–1138
13. Xu X, Lee K, Zhang L, Sonka M, Abramoff MD (2015) Stratified sampling voxel classification for segmentation of intraretinal and subretinal fluid in longitudinal clinical OCT data. IEEE Trans Med Imaging 34(7):1616–1623
14. Harangi B, Hajdu A (2014) Detection of exudates in fundus images using a Markovian segmentation model. In: 36th annual international conference of the IEEE Engineering in Medicine and Biology Society, 2014, vol 2014, pp 130–133
15. Agurto C et al (2014) A multiscale optimization approach to detect exudates in the macula. IEEE J Biomed Health Inform 18(4):1328–1336
16. Sreeja KA, Kumar SS (2019) Comparison of classifier strength for detection of retinal hemorrhages. Int J Innov Technol Exploring Eng 8(6S3):688–693

17. Pradeep A, Joseph XF (2019) Retinal exudate detection using binary operation and hard exudate classification using support vector machine. Int J Innov Technol Exploring Eng 8(9):149–154
18. Arpit S, Singh M (2011) Speckle noise removal and edge detection using mathematical morphology. Int J Soft Comput Eng 1(5):146–149
19. Taghizadeh M, Mahzoun MR (2011) Bidirectional image thresholding algorithm using combined edge detection and P-tile algorithms. J Math Comput Sci 02(02):255–261
20. Rais NB, Hanif MS, Taj IA (2004) Adaptive thresholding technique for document image analysis. In: 8th international multitopic conference, 2004. Proceedings of INMIC 2004, pp 61–66
21. Leedham G, Chen Y, Takru K, Tan JHN, Mian L (2003) Comparison of some thresholding algorithms for text/background segmentation in difficult document images. In: Seventh international conference on document analysis and recognition, 2003. Proceedings, vol 1, pp 859–864
22. Long S, Huang X, Chen Z, Pardhan S, Zheng D (2019) Automatic detection of hard exudates in color retinal images using dynamic threshold and SVM classification: algorithm development and evaluation. Biomed Res Int 2019:1–13
23. Baisantry M, Negi DS, Manocha OP (2012) Change vector analysis using enhanced PCA and inverse triangular function-based thresholding. Def Sci J 62:236–242
24. Akram MU, Tariq A, Khan SA, Javed MY (2014) Automated detection of exudates and macula for grading of diabetic macular edema. Comput Methods Programs Biomed 114(2):141–152
25. Haloi M, Dandapat S, Sinha R (2015) A Gaussian scale space approach for exudates detection, classification and severity prediction. In: ICIP, May 2015
26. Harangi B, Hajdu A (2014) Automatic exudate detection by fusing multiple active contours and regionwise classification. Comput Biol Med 54:156–171
27. Remidio Non-Mydriatic Fundus On Phone (FOP-NM10)
28. Imani E, Pourreza H-R (2016) A novel method for retinal exudate segmentation using signal separation algorithm. Comput Methods Programs Biomed 133:195–205
29. Liu Q, Chen J, Ke W, Yue K, Chen Z, Zhao G (2017) A location-to-segmentation strategy for automatic exudate segmentation in colour retinal fundus images. Comput Med Imaging Graph 55:78–86
30. Rekhi RS, Issac A, Dutta MK, Travieso CM (2017) Automated classification of exudates from digital fundus images. In: 2017 international conference and workshop on bioinspired intelligence (IWOBI), 2017, pp 1–6
31. Fraz MM, Jahangir W, Zahid S, Hamayun MM, Barman SA (2017) Multiscale segmentation of exudates in retinal images using contextual cues and ensemble classification. Biomed Signal Process Control 35:50–62

Chapter 6
Automated Detection of Retinal Hemorrhage Based on Supervised Classifiers and Implementation in Hardware

K. A. Sreeja, S. S. Kumar, and Arun Pradeep

Abstract Supervised machine learning algorithm based retinal hemorrhage detection and classification is presented. For developing an automated diabetic retinopathy screening system, efficient detection of retinal hemorrhage is important. Splat, which is a high level entity in image segmentation is used to mark out hemorrhage in the pre-processed fundus image. Here, color images of retina are portioned into different segments (splats) covering the whole image. With the help of splat level and GLCM features extracted from the splats, two classifiers are trained and tested using the relevant features. The ground-truth is established with the help of a retinal expert and using dataset and clinical images the validation was done. The trained classifier's output is evaluated and the classifier with the best output is chosen for implementation in hardware.

Keywords Retinal hemorrhage · Diabetic retinopathy · Fundus image · Splat feature classification · GLCM features · Raspberry Pi

6.1 Introduction

The World Health Organization estimated that by 2030, there will be nearly 366 million people with Diabetic Mellitus (DM) [1]. A microvascular complication of DM that is responsible for a major share of cases of blindness in the world is the Diabetic Retinopathy (DR). The severe complications like Microaneurysms, Exudates,

K. A. Sreeja (✉)
SCMS School of Engineering and Technology, Ernakulam, India
e-mail: ka.sreeja@gmail.com

S. S. Kumar · A. Pradeep
Noorul Islam University, Kanyakumari, India
e-mail: kumarss@live.com

A. Pradeep
e-mail: arunpradeep@msn.com

Y.-D. Zhang et al. (eds.), *Smart Trends in Computing and Communications: Proceedings of SmartCom 2020*, Smart Innovation, Systems and Technologies 182,
https://doi.org/10.1007/978-981-15-5224-3_6

Occlusion, hemorrhages, etc., together known as DR. The early diagnosis can reduce the risk of losing vision. In order to reduce the diagnosing time, human error and increase the accuracy, several methodologies were developed for early diagnosis of DR and most of them use machine learning techniques. In this paper, classification of hemorrhage and non-hemorrhage fundus images, carried out using two different classifiers is presented. The classifier that performs the best, is chosen for realization in a Raspberry Pi computer system. The techniques used to develop the algorithm was chosen based on recent researches. When compared to large hemorrhages, it is seen that hemorrhages of small size are irregular in shape. Several algorithms were developed to find these abnormalities. In our work one of the classifier decisions is based on Neural network (NN) as described in [2]. Kumar et al. [3] presented a radiomics-driven Computer Aided Diagnosis (CAD) based method. In order to overcome the limitations with current CAD approaches such as decision making a CLass-Enhanced Attentive Response Discovery Radiomics CLEAR-DR is proposed to aid clinical diagnosis of DR. Another important symptom of diabetic retinopathy is exudates, which are similar to hemorrhage pixels. An Early detection of exudates is presented by Wisaeng [4] using Morphology Mean Shift Algorithm (MMSA). Detection of bright and dark lesion which can be hemorrhages or exudates, using a combination of matched filter response(MFR) and Laplacian of Gaussian Response (LoG) [5] produced a 96.10–96.99% accuracy for various publicly available database in hemorrhage detection.Multi-resolution analysis(MRA) is given importance in the work done by Lahmiri [6]. The statistical features obtained after MRA is fed to a support vector machine to grade retinal hemmorhage. Detection of hemorrhage pixels from the bright optical disc is always a constraint. Many methods are already prevailing in order to remove optical disc from the fundus image. Five optic disc detection methods with an algorithms committee having waited voting is presented by Silva et al. [7] where, 6 public benchmark databases with 1566 images are employed. Even though, in our work the optical disc is not removed, this method is useful when pixel based approach is considered. One such method of optic disc removal is used in exudate detection that involves mathematical morphology [8]. After morphological operation, the hard exudates are extracted using adaptive fuzzy logic. The purpose of this research is to develop a supervised classification model using two different classifiers and compare the output based on their sensitivity, specificity and accuracy. Retinal hemorrhages are demarcated with the help of an ophthalmologist who use a high-level representation entity known as splat [9]. Splats are a collection of pixels that have similar fundamental features. A two-step feature selection process is carried out to remove redundant features from the splat and these features are applied to a supervised classification to predict the possibility of hemorrhage splats in the whole image. The hemorrhage is finally detected and shown as bright spots on the dark opponency image. The two classifiers are tested, and their responses are tabulated. Section 6.2 describes the research method. Feature extraction, classification and embedded system realization are portrayed in this section. Section 6.3 gives the result and discussion and Sect. 6.4 summarizes and concludes the work.

6.2 Methodology

After Initial Pre-processing of fundus images by strategies performed in [28, 29] an enhanced image is obtained in which pixels that are assumed to have similar spatial location and share same structural features such as color and intensity are partitioned into non-overlapping splats and spread over the entire image [10]. Splat based method uses several re-sampling strategies. In a fundus image with hemorrhage, the total number of hemorrhage pixels is comparatively less when the entire image is considered [11]. Therefore, a splat-based method is more likely to have better diversity in training the samples. Splats are generated using watershed segmentation algorithm [10]. In order to create meaningful splats, a scale specific over segmentation is performed. This is done in two steps. At first the gradient magnitude of contrast enhanced dark-bright opponent image is taken using different scales. It is done because of the variability in appearance of hemorrhages. All these values are aggregated and the maximum of the gradient value with its scale of interest (SOI) is taken to perform watershed segmentation. Lin et al. [12] The gradient magnitude is computed using Eq. 6.1.

$$|\nabla I(x, y; s)| = \sqrt{I_x(x, y; s)^2 + I_y(x, y; s)^2} \tag{6.1}$$

where $I_x(x, y; s)$ is the image. Now establishing a scale-space representation of the image using Gaussian kernels G_s, the gradient magnitude is calculated from its horizontal and vertical derivative. The maximum of the gradient magnitude is given in Eq. 6.2

$$|\nabla I(x, y)| = \max_i |\nabla I(x, y; s_i)| \tag{6.2}$$

Splats are created using a modified watershed algorithm. The watershed segmented image is shown in Fig. 6.1. All the splats generated throughout the total image area is refrained to a threshold limit. Even though the number of splats increase accuracy, the computation time tends to increase. So a compromise between the efficiency and accuracy has been considered.

6.2.1 Feature Extraction from Splats

After assigning reference labels for splats, a classifier can be trained to detect the target objects. An altogether of 352potentially relevant features are taken to train the classifiers. They are: *Color, Difference Of Gaussian (DoG) Filter, Responses from Gaussian Filter Bank, Responses from Schmid Filter Bank, Responses from Local Texture Filter Banks.* These features are aggregated to obtain a meaningful response image which has low inter splat similarity and high intra splat similarity [13–19].

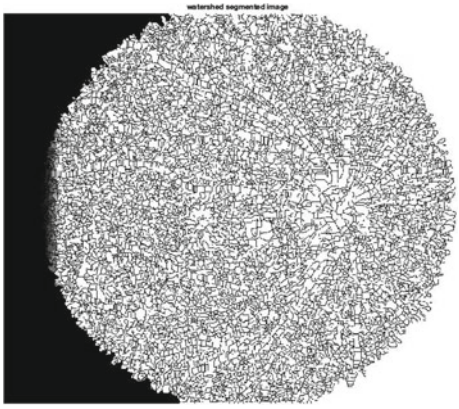

Fig. 6.1 Watershed segmented image

The features mentioned are pixel- based responses. In addition to these features, we take splat wise features according to Gray-Level Co-occurrence Matrix (GLCM) [16–22] statistics.

6.2.2 Preliminary Feature Selection and Classification

A two-step feature selection method is taken here so as to take only the relevant features and discard the irrelevant and redundant ones [23]. The preliminary feature selection is done using a filter approach in order to eliminate the features that are immaterial in discriminating hemorrhage and non-hemorrhage splats. A quadratic discriminant analysis (QDA) [24] is performed and by inspecting the features' variation with Misclassification Error (MCE) [25]. The preliminary features are chosen when the smallest MCE is reached. After preliminary selection, a wrapper approach is performed in order to get an optimal combination of relevant features with minimum redundancy. It is the peculiarity of the wrapper approach that it assesses different combinations of feature subsets customized for a certain classification algorithm with higher computation time [26].The combinations are evaluated using a kNN Classifier. All the selected features are now applied to a sequential forward feature selection subset(SFS). After feature selection, two distinct trained classifiers are set up with the set of features and reference label instances.

kNN and ANN Classification: The kNN algorithm assigns soft class labels. The two classes defined or the outputs are hemorrhage splat or non-hemorrhage splat. The classifier decides the class of a particular splat based on the Euclidean distance of the features in an optimized feature space. The feature vector dimension is 19. As the value of k is increased the computation time increases and the splats are more accurately identified. But since all the k nearest neighbors are not near, an optimum value of k is chosen instead of an arbitrary value. In this work, the value of k is chosen

as 100 with a compromise between computational time and accuracy based on the work in [27]. For ANN, the features are selected that are required to train the neural network. These are the 19 features that were selected by wrapper approach. The neural network is initialized and the number of layers are defined. The weights are assigned arbitrarily small value so as to start the computation. The value of output for each layer is computed and error is calculated. The weights are updated for the output and the hidden layers and is repeated till the all the layers are trained. After training all the layers, it is checked whether all the splat features are used in training purpose. If not the process is repeated until the selection of all splat features is performed. The network is trained τ epochs each time irrespective of whether the network is convergent or not. When the difference of error between the current training series and the previous series is smaller than a threshold , then it can be concluded that the network is convergent and the training is stopped. After the training is completed, the classifier is validated for its accuracy using the validation set. The validation set does not change the trained values of the classifier and it is done only to ensure that overfitting has not occurred. To determine the class of splat sigmoid transfer function $S(x) = \frac{1}{1+e^{-x}}$ is used. When $S(x) = 1$ then it comes under a hemorrhage splat and when $S(x) = 0$, it is a non-hemorrhage splat.

6.3 Results and Discussions

Histogram equalization is done using the strategy proposed in [28, 29]. Also each image is normalized according to its prevailing pixel value at the three colour channels. The pixel values that occur frequently are shifted to the beginning of RGB colour space. Among the total of 1500 images obtained from from the publically available database DIARETDB1 and the clinical images from Dr. Bhejan Singh's eye hospital, Nagercoil, 1050 were taken for training, 225 images for testing and 225 for validation. 10,500 splats were created among which 300 are hemorrhage splats. Images with at least 6 splats are taken for training. After sequential forward feature selection subset (SFS) only the relevant features were considered whereas the insignificant and redundant ones were removed from the feature set. The final feature set consists of 50 features from the 352 features obtained by filter approach and from this set 19 features were finally obtained by wrapper approach. The details of the final selected features are given in Table 6.1.

6.3.1 Classification of Splats Using kNN and ANN Classifiers

The splats are represented as a 19 dimensional feature vector. The kNN classifier and the ANN Classifier are trained on these features. Different values of k were tested whose values are chosen between 15 and 160 that involves both feature selection as well classification. After repeated iterations, the value of k was fixed at 100 without

Table 6.1 Details of final selected features

Features	Number	Description
DoG filter bank	s2–s0.5	From Green channel
DoG filter bank	s4–s0.5	From db and rg opponency
DoG filter bank	s8–s0.5	From db opponency
Gaussian filter bank	s = 8 orientation: 2, 3	Mean of second order Gaussian derivative from green channel
Gaussian filter bank	s = 1, 2, 4 orientation: 1, 2, 3	Mean of second order Gaussian derivative from green channel
Schmid filter bank	Response = 11	From db opponency
Mean of Gaussian	s = 8, 16	From Green channel

compromising the computation time and prediction accuracy. The target class for the classifier or the output consists of two classes: Hemorrhage or Non-Hemorrhage. The two classifiers were tested with the equal number of images and the results were compared. The splat centered Region of Convergence (ROC) curve for the fundus image given in Fig. 6.2 using the two classifiers are shown in Figs. 6.3 and 6.4. For a fundus image with 469 splats, the level of accomplishment of these classifiers are represented in the ROC curve. From the ROC curve for various threshold values, it is found that, among the two, ANN outperforms kNN classifiers in terms of sensitivity with an Area Under Curve (AUC) of 0.80 than 0.75 of kNN classifier. The confusion matrix calculated is given in Figs. 6.5 and 6.6 where n denotes the total number of splats for 520 images. A total 22574 splats were identified from the 520 images and they provide different accuracy at a certain threshold. The best classifier that performed in evaluation which is the ANN is now chosen for implementation in hardware.

6.3.2 Implementation in Hardware

Image preprocessing, processing and classification was done in MATLAB using Intel i5 dual-core processor which has 8 GB RAM memory specification and a clock speed of 1.6 GHz. The motivation behind this work was to develop an aid to assist medical practitioners for an early and accurate diagnosis of DR. An easy diagnosis is accomplished if the whole process of detection was implemented on an integrated hardware. The tested and successfully executed algorithms were then implemented in Raspberry-Pi system as seen in Fig. 6.7. The inclination towards Raspberry-Pi board is the ease of designing a portable convenient handheld device. The Mobile Industry Processor Interface (MIPI) interface is connected to a fundus camera by which the real time images can be directly processed to detect hemorrhages which

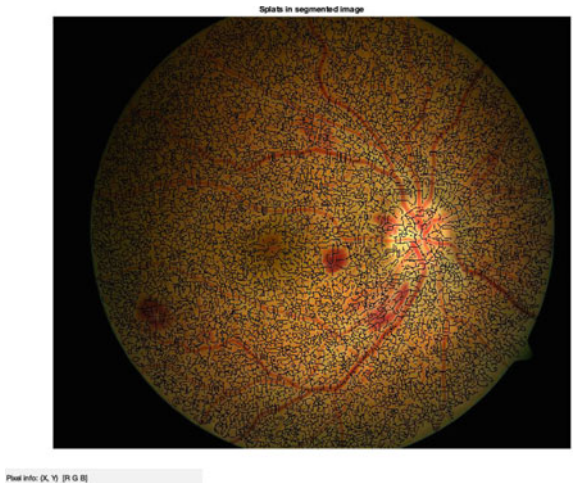

Fig. 6.2 Splats identified

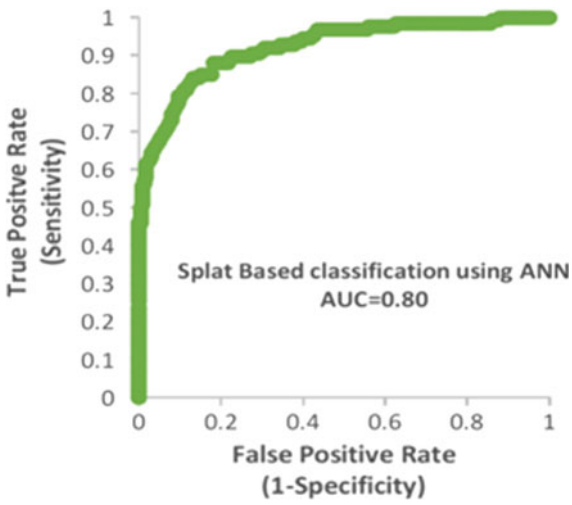

Fig. 6.3 ROC for ANN

can predict the possibility of DR. This system can also be used with the help of a smart-phone camera and an aspheric lens to capture retinal images. Two Fundus

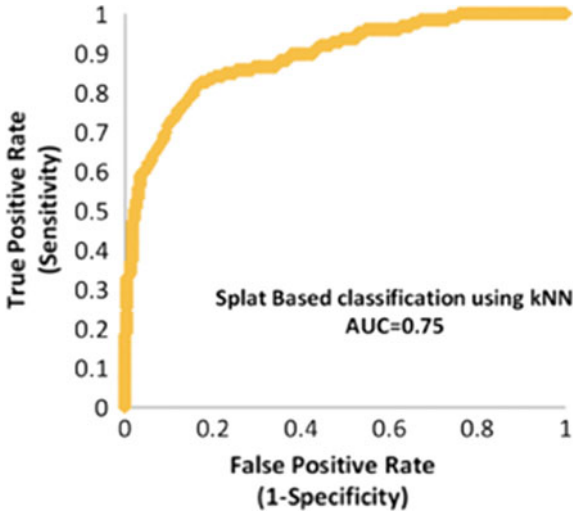

Fig. 6.4 ROC for kNN

n= 18892	Predicted NO	Predicted YES	
Actual NO	TN= **9246**	FP=**202**	9548
Actual YES	FN= **669**	TP=**8775**	9344
	9915	8977	

Fig. 6.5 Confusion matrix for ANN

n=**22574**	Predicted NO	Predicted YES	
Actual NO	TN= **11257**	FP=**139**	11396
Actual YES	FN= **720**	TP=**10458**	11178
	11977	10597	

Fig. 6.6 Confusion matrix for kNN

images 1 and 2 were taken from standard diabetic retinopathy database DIARETDB1 and from clinical database for testing. Figures 6.8 and 6.9 shows the various stages of hemorrhage detection on images obtained from these source.

6.4 Conclusion

The presented work is a novel technique to detect exudates using morphological operation. The new enhancement method IIHE was used to increase the sensitivity of our existing algorithm that originally involved enhancement using CLAHE. A considerable increase in specificity indicates that the algorithm is more accurate while considering low intensity images. Using the same feature set to the classifier, the score of evaluation parameters could be increased by changing the enhancement technique. Further studies can be implicated to increase the PPV and F-Score of this algorithm. Thus a splat-based feature classification using Raspberry Pi is presented for the detection of retinal hemorrhage. The proposed classification strategy can model different lesions with different texture size and appearance. The algorithm is

Fig. 6.7 Raspberry Pi implementation

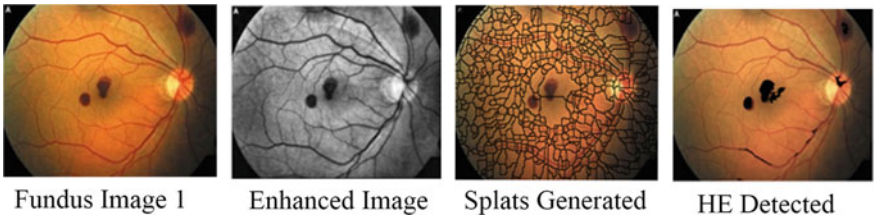

Fig. 6.8 Hemorrhage detection process applied on DIARTEDB1 fundus image

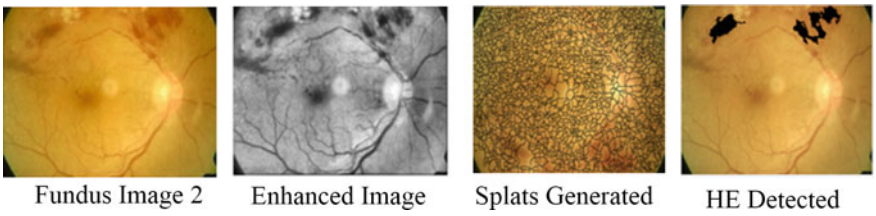

Fig. 6.9 Hemorrhage detection process applied on Clinical fundus image

validated on the publically available database DIARETDB1 and clinical image which was captured using a "Remidio Non-Mydriatic Fundus on Phone (FOP-NM10). The proposed detector can be incorporated into comprehensive DR assisting system for ophthalmologists.

References

1. World Health Organization: Prevent ion of blindness from diabetes mellitus (2006)
2. Zeng, X., Chen, H., Luo, Y., Ye, W.: Automated diabetic retinopathy detection based on binocular siamese-like convolutional neural network. IEEE Access **7**, 1 (2019)
3. Kumar, D., Taylor, G.W., Wong, A.: Discovery radiomics with CLEAR-DR: interpretable computer aided diagnosis of diabetic retinopathy. IEEE Access **7**, 25891–25896 (2019)
4. Wisaeng, K., Sa-Ngiamvibool, W.: Exudates detection using morphology mean shift algorithm in retinal images. IEEE Access **7**, 11946–11958 (2019)
5. Kar, S.S., Maity, S.P.: Automatic detection of retinal lesions for screening of diabetic retinopathy. IEEE Trans. Biomed. Eng. **65**(3), 608–618 (2018)
6. Lahmiri, S.: High-frequency-based features for low and high retina haemorrhage classification. Healthc. Technol. Lett. **4**(1), 20–24 (2016)
7. Silva, R.R.V.E., De Araújo, F.H.D., Dos Santos, L.M.R., Veras, R.M.S., De Medeiros, F.N.S.: Optic disc detection in retinal images using algorithms committee with weighted voting. IEEE Lat. Am. Trans. **14**(5), 2446–2454 (2016)
8. Ranamuka, N.G., Meegama, R.G.N.: Detection of hard exudates from diabetic retinopathy images using fuzzy logic. IET Image Process. **7**(2), 121–130 (2013)
9. Tang, L., Niemeijer, M., Reinhardt, J.M., Member, S., Garvin, M.K., Abrà moff, M.D.: Splat feature classification with application to retinal hemorrhage detection in fundus images. IEEE Trans. Med. Imaging **32**(2), 364–375 (2013)
10. Fairfield, J.: Toboggan contrast enhancement for contrast segmentation. In: 1990 10th International Conference on Pattern Recognition, vol. 1, pp. 712–716 (1990)
11. Chawla, N.V., Japkowicz, N., Ko, A.: Editorial: special issue on learning from imbalanced data sets. SIGKDD Explor. Newsl. **6**, 1–6 (2004). https://doi.org/10.1145/1007730.1007733
12. Lin, Y.-C., Tsai, Y.-P., Hung, Y.-P., Shih, Z.-C.: Comparison between immersion-based and toboggan-based watershed image segmentation. IEEE Trans. Image Process. **15**(3), 632–640 (2006)
13. Abraoff, M.D., et al.: Automated segmentation of the optic disc from stereo color photographs using physiologically plausible features. Investig. Opthalmology Vis. Sci. **48**(4), 1665 (2007)
14. Romeny, B.M.: Front-End Vision and Multi-scale Image Analysis: Multi-scale Computer Vision Theory and Applications, 1st edn. Springer, Berlin (2003)

15. Tang, L., Niemeijer, M., Abramoff, M.D.: Splat feature classification: detection of the presence of large retinal hemorrhages. In: 2011 IEEE International Symposium on Biomedical Imaging: From Nano to Macro, pp. 681–684 (2011)
16. Engler, O.: Introduction to Texture Analysis: Macrotexture, Microtexture, and Orientation Mapping, 2nd edn. CRC Press LLC, Boca Raton (2017)
17. Varma, M., Zisserman, A.: A statistical approach to texture classification from single images. Int. J. Comput. Vis. **62**(1/2), 61–81 (2005)
18. Alharan, A.F.H., Fatlawi, H.K., Ali, N.S.: A cluster-based feature selection method for image texture classification. Indonesian J. Electr. Eng. Comput. Sci. **14**(3), 1433–1442 (2019)
19. Hasan, A.M.: A hybrid approach of using particle swarm optimization and volumetric active contour without edge for segmenting brain tumors in MRI scan. Indonesian J. Electr. Eng. Inform. **6**(3), 292–300 (2018)
20. Tamura, H., Mori, S., Yamawaki, T.: Textural features corresponding to visual perception. IEEE Trans. Syst. Man. Cybern. **8**(6), 460–473 (1978)
21. Niemeijer, M., Staal, J., van Ginneken, B., Loog, M., Abramoff, M.D.: Comparative study of retinal vessel segmentation methods on a new publicly available database. In: Proceedings of the SPIE 5370, Medical Imaging 2004: Image Processing (12 May 2004). https://doi.org/10.1117/12.535349
22. Niemeijer, M., Abramoff, M.D., van Ginneken, B.: Segmentation of the optic disc, macula and vascular arch in fundus photographs. IEEE Trans. Med. Imaging **26**(1), 116–127 (2007)
23. Kohavi, R., John, G.H.: Wrappers for feature subset selection. Artif. Intell. **97**(1–2), 273–324 (1997)
24. Srivastava, S., Gupta, M.R., Frigyik, B.A.: Bayesian quadratic discriminant analysis. J. Mach. Lear. Res. **8**, 1277–1305 (2007)
25. Duda, R.O., Hart, Peter E., Stork, D.G.: Pattern Classification, 2nd edn. Wiley, Hoboken (2000)
26. Tarassenko, L., Roberts, S.: Supervised and unsupervised learning in radial basis function classifiers. IEE Proc. Vis. Image Signal Process. **141**(4), 210–216 (1994). https://doi.org/10.1049/ip-vis:19941324
27. Sreeja, K.A., Kumar, S.S.: Comparison of classifier strength for detection of retinal hemorrhages. Int. J. Innovative Technol. Exploring Eng. (IJITEE.org) **8**(S63), 688–693 (2019)
28. (9) (2019)
29. Arun, P., Felix, J.X.: Intensity index based histogram equalization technique for retinal image enhancement and classification of hard exudates using supervised learning. Int. J. Eng. Adv. Technol. (IJEAT.org) **8**(5) (2019)

Back

MOBICOM

Intelligent vehicle collision avoidance system using 5G-enabled drone swarms

Authors: Sunil Jacob, Varun G Menon, Parvathi R, Shynu P G, Fathima Shemim KS, Bandana Mahapatra, Mithun Mukherjee Authors Info & Claims

DroneCom '20: Proceedings of the 2nd ACM MobiCom Workshop on Drone Assisted Wireless Communications for 5G and Beyond
• September 2020 • Pages 91–96 • https://doi.org/10.1145/3414045.3415938

Published: 07 October 2020 Publication History Check for updates

ABSTRACT

The number of vehicular collisions is on a toll worldwide. Despite enforcing stringent laws and incorporating various safety features, the causalities are still on the rise. Existing techniques such as vision zero strategy and safe system approach provides only post-crash aid. Although numerous works have been carried out on Intelligent Transportation Systems (ITS), a well-coordinated vehicular collision avoidance system is still missing. In this paper, we utilize the tremendous opportunity provided by ITS, Light Detection and Ranging (LIDAR), Wireless Sensor Networks (WSN), 5G, and propose an effective system using drones with swarm intelligence that can automatically control the

Back

networks and always ensures a safe distance between the vehicles using the principle of magnetic levitation. The system is further investigated for optimizing the power, altitude, and angular

MOBICOM

References

1. Zhao, J., Xu, H., Liu, H., Wu, J., Zheng, Y. and Wu, D., 2019. Detection and tracking of pedestrians and vehicles using roadside LiDAR sensors. *Transportation research part C: emerging technologies*, 100, 68--87.

2. Abbasi, M. et al., 2020. An efficient parallel genetic algorithm solution for vehicle routing problem in cloud implementation of the intelligent transportation systems. *Journal of Cloud Computing* 9, 1, 1--14.

3. Garg, S. et al., 2019. SDN-based secure and privacy-preserving scheme for vehicular networks: a 5G perspective. *IEEE Transactions on Vehicular Technology* 68, 9, 8421--8434.

Show All References

Cited By

View all

Wang H, Jiang J, Huang G, Wang W, Deng D, Elhalawany B, Li X and Ye Y. (2022). Physical Layer Security of Two-Way Ambient Backscatter Communication Systems. *Wireless Communications & Mobile Computing*. **2022**. Online publication date: 1-Jan-2022.

https://doi.org/10.1155/2022/5445676

Li X, Zheng Y, Khan W, Zeng M, Li D, Ragesh G and Li L. Physical Layer Security of Cognitive Ambient Backscatter Communications for Green Internet-of-Things. *IEEE Transactions on Green Communications and Networking*. 10.1109/TGCN.2021.3062060. **5**:3. (1066-1076).

https://ieeexplore.ieee.org/document/9363336/

Back

https://ieeexplore.ieee.org/document/9409837/

MOBICOM

Index Terms

Intelligent vehicle collision avoidance system using 5G-enabled drone swarms

Computer systems organization

Networks

Dependable and fault-tolerant systems and networks

Network architectures

Recommendations

A lane-level cooperative collision avoidance system based on vehicular sensor networks
MobiCom '13: Proceedings of the 19th annual international conference on Mobile computing & networking

Read More

Acceptance and Effectiveness of Collision Avoidance System in Public Transportation
Design, User Experience, and Usability: Users, Contexts and Case Studies

Read More

Context-Aware Cooperative Collision Avoidance Vehicle Braking Alert System for VANET
ICCASA '14: Proceedings of the 3rd International Conference on Context-Aware Systems and Applications

Read More

Comments

< Back

Comments should be relevant to the contents of this article, (sign in required).

Got it

MOBICOM

0 Comments

Share **Best** **Newest** **Oldest**

Nothing in this discussion yet.

View Table Of Contents

Back

MOBICOM

Morphological Operators on Hypergraphs for Colour Image Processing

Bino Sebastian V*
Department of Mathematics
Mar Athanasius College
Kothamangalam
binosebastianv@gmail.com

Nuja M Unnikrishnan
Department of Basic Science and Humanities
SCMS School of Engineering and Technology
Karukutty
nuja@scmsgroup.org

Neenu Sebastian
Dept. of Computer Science and Engineering
SCMS School of Engineering and Technology
Karukutty
neenusebastian@scmsgroup.org

Rosebell Paul
Dept. of Computer Science and Engineering
SCMS School of Engineering and Technology
Karukutty
rosebell@scmsgroup.org

***Abstract*—This article is an extension of morphological operators on hypergraphs to work with colour images. Morphological operators on hypergraphs are useful for binary and grayscale image processing. The preliminary experimental results related to the extension of these operators to colour images is presented in this paper. The results on colour images are promising and is a better alternative for the existing methods.**

***Index Terms*—Hypergraph, Mathematical Morphology, Image Processing, Salt and pepper noise.**

I. Introduction

Mathematical morphology is the first consistent non-linear image analysis theory. Originally it was defined on a set theoretic framework and used for processing binary images and extended to grayscale images. Despite its continuous origin, it was soon recognised that the roots of the theory were in algebraic theory, notably the framework of complete lattices. This allows the theory to be completely adaptable to non-continuous spaces, such as graphs [4], hypergraphs [3] and simplicial complexes [5]. Extending Mathematical Morphology to colour images is an active area of research in image processing [8, 18, 9]. There is no natural extension of the morphological operators to colour images. This is because colour images does not admit a partial ordering [11]. Image denoising is one of the most important operations in image processing. Salt and pepper noise is very common in image processing applications and noise reduction is a very active area of research in this field [12]. Morphological filtering is one of the most reliable techniques for salt and pepper noise reduction [2, 4, 5]. Our objective is to utilise the morphological operators defined on hypergraphs to remove this noise from colour iamges [2, 16].

*This work is supported by RUSA, Govt. of India under the MRP scheme.

978-1-7281-6453-3/20/$31.00 ©2020 IEEE

This article is organised as follows. We introduce the preliminary definitions from mathematical morphology and morphological operators on hypergraphs in section II. In Section III, we present the hypergraph representation of a digital image. Experimental results of the operators and filters on a colour image are presented in Section IV. Conclusion and future works are presented in Section V.

II. Preliminaries

A. Mathematical Morphology

Definition 1. [6, 7, 14, 17] Given two lattices $\mathcal{L}_1$ and $\mathcal{L}_2$, any operator $\delta : \mathcal{L}_1 \to \mathcal{L}_2$ that distributes over the supremum and preserves the least element is called a dilation. An operator that distributes over the infimum and preserves the greatest element is called an erosion.

Definition 2. [6, 7, 14] Two operators $\varepsilon : \mathcal{L}_1 \to \mathcal{L}_2$ and $\delta : \mathcal{L}_2 \to \mathcal{L}_1$ form an adjunction (ε, δ) if for any $X \in \mathcal{L}_2$ and any $Y \in \mathcal{L}_1$, we have $\delta(X) \leq_1 Y \Leftrightarrow X \leq_2 \varepsilon(Y)$, where $\leq_1$ and $\leq_2$ denote the order relations in $\mathcal{L}_1$ and $\mathcal{L}_2$ respectively.

Definition 3. [6, 7, 17] Let δ be any operator on a lattice $\mathcal{L}$, then δ is

- increasing if $X \leq Y$ implies $\delta(X) \leq \delta(Y)$;
- extensive if $\delta(X) \geq X$ for every $X \in \mathcal{L}$;
- anti extensive if $\delta(X) \leq X$ for every $X \in \mathcal{L}$;
- idempotent if $\delta^2 = \delta$;
- a morphological filter if δ is increasing and idempotent;
- an opening if δ is increasing, anti-extensive and idempotent;
- a closing if δ is increasing, extensive and idempotent.

B. Morphological operators on hypergraphs

A hypergraph is denoted as a pair $H = (H^\bullet, H^\times)$ where $H^\bullet$ is a set and $H^\times$ is a family $(e_i)_{i\in I}$ of nonempty subsets of $H^\bullet$. Let X and Y be two hypergraphs. If $X^\bullet \subseteq Y^\bullet$ and $X^\times \subseteq Y^\times$, then X is a subhypergraph of Y and is denoted by $X \subseteq Y$. Let $H = (H^\bullet, H^\times)$ be a hypergraph and consider

the sets $\mathcal{H}^\bullet$,$\mathcal{H}^\times$ and $\mathcal{H}$ of respectively all subsets of $H^\bullet$, all subsets of $H^\times$ and all subhypergraphs of $\mathcal{H}$[2, 16]. The vertex-hyperedge correspondence defined in [2,16] by the operators $\delta^\bullet$, $\epsilon^\bullet$ from $\mathcal{H}^\times$ into $\mathcal{H}^\bullet$ and $\delta^\times$, $\epsilon^\times$ from $\mathcal{H}^\bullet$ into $\mathcal{H}^\times$ act as the building blocks for morphological operators on hypergraphs. These operators are used to process colour images in this work.

Definition 4 [2]

- Vertex dilation $\delta = \delta^\bullet \circ \delta^\times$ and vertex erosion $\epsilon = \epsilon^\bullet \circ \epsilon^\times$.
- Opening $\gamma_1 = \delta \circ \epsilon$ and closing $\phi_1 = \epsilon \circ \delta$.
- Half opening $\gamma_{1/2} = \delta^\bullet \circ \epsilon^\times$ and half closing $\phi_{1/2} = \epsilon^\bullet \circ \delta^\times$.

Property 1. If $X^\bullet \subseteq H^\bullet$, then $\gamma_1(X^\bullet) \subseteq \gamma_{1/2}(X^\bullet) \subseteq X^\bullet \subseteq \phi_{1/2}(X^\bullet) \subseteq \phi_1(X^\bullet)$.

Property 2. The operators $\gamma_{1/2}$ and γ_1 are openings on $\mathcal{H}^\bullet$ and $\phi_{1/2}$ and ϕ_1 are closings on $\mathcal{H}^\bullet$.

C. Flat morphological operators on weighted hypergraphs

Let n denote any positive integer and K = $\{0, \ldots, n\}$.Let E be any set. Let *Fun(E)* denote the set of all maps from E to K. By threshold decomposition [2], the lattice $\mathcal{H}$ of all subhypergraphs of *H* induces a lattice $\mathrm{Fun}(H^\bullet) \otimes \mathrm{Fun}(H^\times)$ of pairs of functions weighting respectively the vertices and the hyperedges of *H* such that the simultaneous threshold of these two functions at any given level yields a subhypergraph of *H*.

The operators acting on the lattices $\mathcal{H}^\bullet$,$\mathcal{H}^\times$ or $\mathcal{H}$ are all increasing and, they induce stack operators [1, 10, 13, 15, 19] acting on the lattices $\mathrm{Fun}(H^\bullet)$, $\mathrm{Fun}(H^\times)$, and $\mathrm{Fun}(H^\bullet) \otimes \mathrm{Fun}(H^\times)$. This implies that the properties presented for hypergraph operators on the lattices $\mathcal{H}^\bullet$,$\mathcal{H}^\times$ or $\mathcal{H}$ also hold good for operators on the lattices $\mathrm{Fun}(H^\bullet)$, $\mathrm{Fun}(H^\times)$, and $\mathrm{Fun}(H^\bullet) \otimes \mathrm{Fun}(H^\times)$.

The following definition is the stack analougues to the operators $\delta^\bullet$, $\epsilon^\times$,$\epsilon^\bullet$,$\delta^\times$ on weighted hypergraphs [2].

Definition 5 [2] Let $F^\bullet \in \mathrm{Fun}(H^\bullet)$ and let $F^\times \in \mathrm{Fun}(H^\times)$

- $\delta^\bullet(F^\times)(x) = max_{x \in v(e_i)}\{F_\times(e_i) | e_i \in H^\times\} \forall x \in H^\bullet$
- $\epsilon^\times(F^\bullet)(e_i) = min\{f^\bullet(x) | x \in v(e_i)\} \forall e_i \in H^\times$
- $\epsilon^\bullet(F^\times)(x) = min_{x \in v(e_i)}\{F_\times(e_i) | e_i \in H^\times\} \forall x \in H^\bullet$
- $\delta^\times(F^\bullet)(e_i) = max\{f^\bullet(x) | x \in v(e_i)\} \forall e_i \in H^\times$

This idea is used to define Alternating Sequential Filters on binary and grayscale images represented as uniform hypergraphs. The same idea can be extended to be utilised for colour images also. Further it can also be used to define ASFs on colour images by suitable choice of a partial order on colour images.

III. Colour Image Representation

We represent the RGB components of a colour image by means of a vertex weighted hypergraph. Each pixel correspond to the vertices of the hypergraph and the weights are assigned according to the intensity values of the corresponding pixels. We use the 3-uniform hypergraph presented in Figure 1 to represent the hyperedges. This is because this structure gives the best results for binary and grayscale image filtering

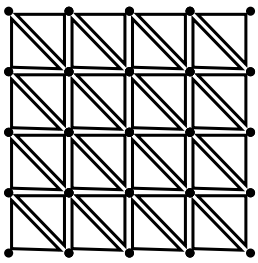

Fig. 1: Hypergraph structure used to represent an image.

applications. The vertex weights are propogated along the hyperedges to obtain the morphological operators, thereby producing the component images [2]. The component images are then combined to generate the resultant colour image.

IV. Experimental Results

The definitions and results presented in the previous sections are used to obtain the dilated and eroded colour images. This is achieved by propagating the vertex weights of the hypergraphs along its hyperedges to obtain the flat morphological operators presented in [2]. Composition of these operators produce the resultant images to generate half opened $(\gamma_{1/2})$ half closed $(\phi_{1/2})$, opened (γ_1) and closed (ϕ_1) images as shown in 2 (c) to (f).

By property 1, half opening and half closing of the vertex set of a hypergraph are more close to the original vertex set than that of opening and closing. Moreover both of them are filters and capable of removing noise from the image, where the image is represented as a hypergraph. In this paper we utilise this idea on colour images to illustrate the effectiveness of these operators.

Figure 2(a) is a colour image taken from [11]. The noisy version of this image added with salt and pepper noise is shown in Figure 2(b). The mean square error (MSE) for this image is 32.72%. The half opened $(\gamma_{1/2})$ image is shown in Figure 2(c). Almost all the salt kind of noise is removed by this operation and causes less damage to the image. Figure 2(d) shows the half closed $(\phi_{1/2})$ image in which the pepper noise is almost completely removed. Figure 2 (e) and (f) shows the results of opening (γ_1) and closing (ϕ_1) of (b) respectively. Here also the noise is removed but the damage caused to the image is more compared to the previous cases. The composition $(\gamma_{1/2}) \circ (\phi_{1/2})$ or half closing followed by half opening is an alternating sequential filter (ASF) and capable of removing impulse noise effectively from binary and grayscale images [2]. The result of this operation on the tested colour image in Figure 2(b) is shown in Figure 3(b). The mean square error is reduced to 2.75% in this case. The open-close filter $(\gamma_1) \circ (\phi_1)$ reduces the mean square error to 3.57%. This is shown in Figure 3(a).

Experimental results shows that the resultant colour images obtained by half opening and half closing are better than the images obtained by opening and closing operations. This is because half opening and half closing are better approximations to the original image and cause less damage to the image

(a) Original Image

(b) Noisy version MSE = 32.72%

(c) Half Opening

(d) Half Closing.

(e) Opening.

(f) Closing.

Fig. 2: Illustration of the operators on a colour image.

(a) $\gamma_1 \circ \phi_1 MSE = 3.57\%$

(b) $\gamma_{1/2} \circ \phi_{1/2} MSE = 2.75\%$

Fig. 3: Illustration of colour image filtering.

than opening and closing. Thus half opening and half closing can be used more effectively than opening and closing for colour image denoising. In this work we do not use any partial ordering of colour vectors.

V. Conclusion and future works

The objective of this study is to identify the possibilities of using morphological operators on hypergraphs for colour image processing. Morphological operations like half opening and half closing are not at all possible using traditional morphological image processing using structuring elements. Graph and hypergraph structures to represent digital images allows this kind of operations. The results are required to be tested on a large dataset of colour images inorder to validate the consistency of the proposed method. The initial results are promising and the future works are directed towards a more suitable hypergraph representation of colour images incorporating partial ordering on the colour components. The possiblility of false colours in morphological colour image processing is not completely removed in this method but the effect of which is minimized. Use of partial ordering of colours on hypergraphs is a solution for this problem.

References

[1] Gilles Bertrand, "On topological watersheds," in Journal of Mathematical Imaging and Vision, vol. 22(2-3), pp.217–230 , 2005.

[2] Kannan Balakrishnan Bino Sebastian Vadakkenveettil, Avittathur Unnikrishnan and Ramkumar Padinjare Pisharath Balakrishna," Morphological filtering on hypergraphs", in Discrete Applied Mathematics, 216 pp.307–320,2017.

[3] Isabelle BLOCH and Alain BRETTO, "Mathematical morphology on hypergraphs, application to similarity and positive kernel," in Computer vision and image understanding, vol. 117(4), pp.342-354 2013.

[4] Jean Cousty, Laurent Najman, Fabio Dias, and Jean Serra, "Morphological filtering on graphs," Computer Vision and Image Understanding,vol. 117(4), pp.370–385 , 2013.

[5] Fabio Dias, Jean Cousty, and Laurent Najman, “Dimensional operators for mathematical morphology on simplicial complexes,” in Pattern Recognition Letters, 2014.
[6] Henk JAM Heijmans.a, “Composing morphological filters,” IEEE Transactions on Image processing,vol. 6(5), pp.713–723 , 1997.
[7] Henk JAM Heijmans and Christian Ronse,”The algebraic basis of mathematical morphology i. dilations and erosions”,Computer Vision, Graphics, and Image Processing,vol.50(3),pp.245–295,1990
[8] J. B. T. M. Roerdink J. J. van de Gronde, “Group-invariant colour morphology based on frames.,” IEEE Transactions on Image Processing, vol. 23(3), pp.12761288 , 2014.
[9] Yao Wu Yong Li Jing Hu JunpingWang, Gangming Liang, “New colour morphological operators on hypergraph,” IET Image Processing,, vol. 12, pp.690–695 , May 2018.
[10] Romain Lerallut, Etienne Decenci‘ere, and Fernand Meyer, “Image filtering using morphological amoebas,” Image and Vision Computing, vol.25(4) , pp.395–404 , 2007.
[11] Olivier Lezoray, “Manifold-based mathematical morphology for graph signal editing of colored images and meshes”,In IEEE International Conference on Systems, Man, and Cybernetics (SMC 2016), Budapest, Hungary, October 2016.
[12] Mehdi Mafi, Harold Martin, Mercedes Cabrerizo, Jean Andrian, Armando Barreto, and Malek Adjouadi.,”A comprehensive survey on impulse and gaussian denoising filters for digital images.”,Signal Processing,,vol.157,pp.236–260,2019
[13] Petros Maragos and Ronald W Schafer,”Morphological filterspart i: Their set-theoretic analysis and relations to linear shift-invariant filters”,in IEEE Transactions on Acoustics, Speech and Signal Processing,vol.35(8),pp.11531169,1987.
[14] Laurent Najman and Hugues Talbot,“Mathematical Morphology.,” John Wiley and Sons, 2013
[15] Christian Ronse, “Flat morphology on power lattices,” Journal of Mathematical Imaging and Vision,vol. 26(1-2), pp.185–216 , 2006.
[16] Bino Sebastian, A Unnikrishnan, Kannan Balakrishnan, and PB Ramkumar, “Mathematical morphology on hypergraphs using vertex-hyperedge correspondence,”ISRN Discrete Mathematics, 2014.
[17] Jean Serra., “Lecture notes on morphological operators.,”Mittag-Lefflers matematiska stiftelse, 2014.
[18] Marcos Eduardo Valle and Raul Ambrozio Valente,”Mathematical morphology on the spherical cielab quantale with an application in color image boundary detection”,in Journal of Mathematical Imaging and Vision,vol.57,pp.183201,2016
[19] P Wendt, Edward J Coyle, and Neal C Gallagher Jr. Stack filters,IEEE Transactions on Acoustics, Speech and Signal Processing,vol.34(4),pp.898911,1986

PERSPECTIVES ON CONTEMPORARY LITERATURE AND LITERARY THEORIES IN ENGLISH

Editor :
Prof. P. Kannan

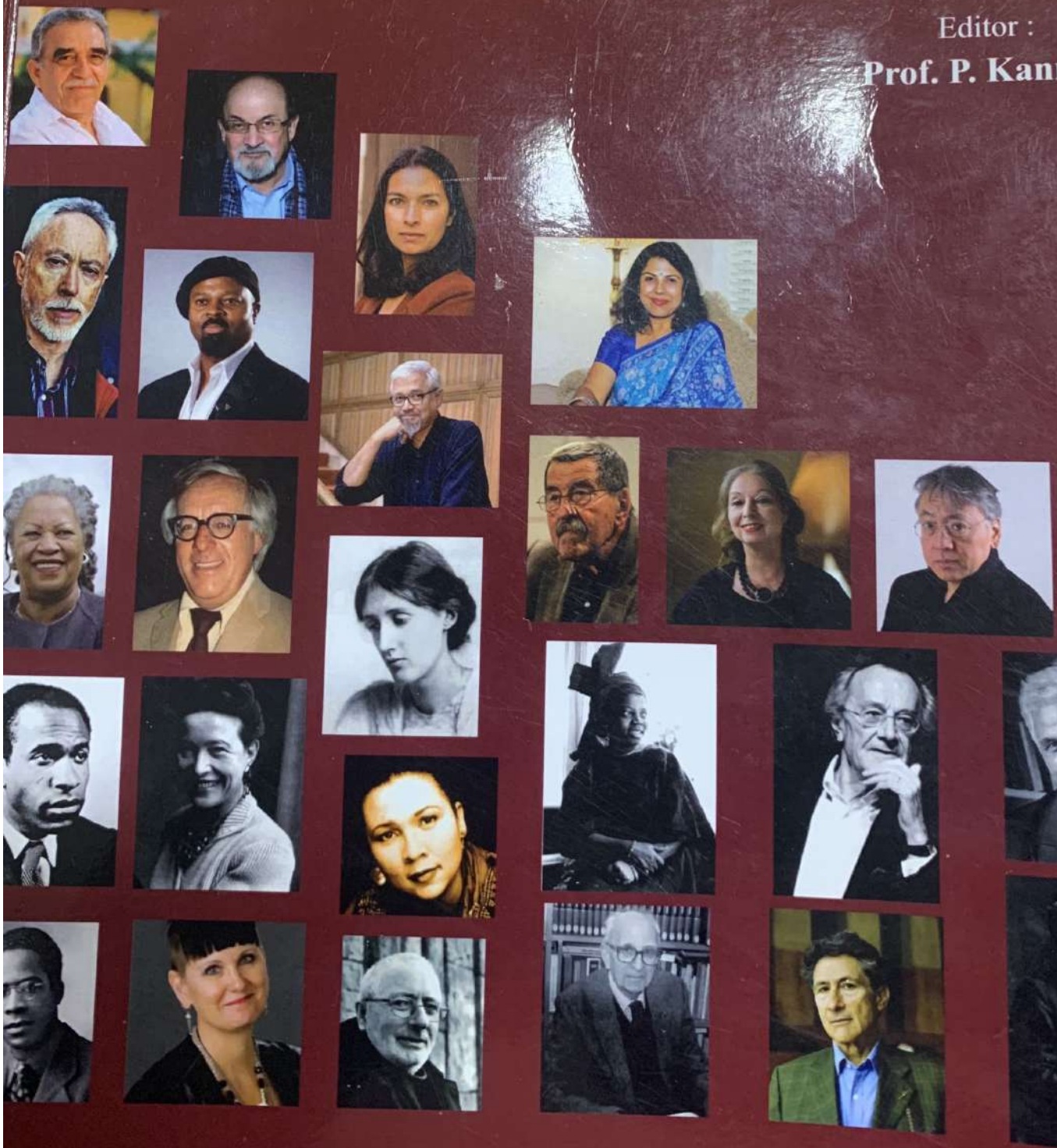

PERSPECTIVES ON CONTEMPORARY LITERATURE AND LITERARY THEORIES IN ENGLISH

Editor :

Prof. P. Kannan

Published by :

Jeevan Publication

Bhadravathi-577301

Pages : 345 Page

Price : Rs. 500-00

ISBN : 9789388551052-01130

Printed by :

Sri Malleshwara Printers & Enterprises

C. N. Road, Bhadravati.

Living in the Wilderness

Jane Theresa
Assistant Professor
SCMS School of Engineering and Technology
Kerala
jane@scmsgroup.org
8547731698

Abstract

Nature makes us feel alive and energetic. It has the power to bring our mind, body, and soul back to life. Nature's healing powers are absolutely amazing. It is therapeutic for everyone and is open to both the rich and the poor. Recognizing Nature's healing power, many people travel to places around the world that offer consolation and comfort. Nature is not just around us, it's within us as well. This provides an unexplained sense of calm consciousness. Several studies are now available that show nature's psychological benefits. All the research points the fact that the closer we find ourselves to nature, the happier we feel. Nature is, in fact, a strong antidepressant.

The paper is about the consoling power of nature experienced by the characters when they are in the natural settings in the novel *The Tree of Man* written by Patrick White. The study is an eco-psychological re-reading of the text which will allow readers to witness how the environment becomes an inevitable part of human life that reflects the interconnectedness of all that the nature has created. The escape to nature has another appeal besides its beauty and tranquillity. Ecological interactions touch an individual's physical, spiritual, emotional and psychological facets of life. Eco psychology is a modern social and intellectual movement aimed at recognizing and harmonizing the relationship between people and the Earth. The emerging field of eco-psychology shows how our human psyches are closely bound to the elemental earth.

Earth centred faiths strives to honour the strength of nature's consoling power. This eco psychological study shows how the text demonstrates the character's harmonious and balanced eco human bonding. It shows how far identities of characters are shaped by the surroundings in which they live. The study describes how the ecological lifestyle is an encompassing transformation that touches every facets of an individual's life. The experiences encountered by the characters in the novel shows how the experiences in life with the natural environment move them towards a greater appreciation and concern for the natural world. Thus the paper studies *The Tree of Man* as an ecological writing with a literature of hope.

Keywords-

Eco criticism, Biophilia, Eco psychology, Self revelation

Living in the Wilderness

I wandered lonely as a cloud
That floats on high o'er vales and hills,
When all at once I saw a crowd,
A host, of golden daffodils;
Beside the lake, beneath the trees,
Fluttering and dancing in the breeze.

(William Wordsworth)

The paper is about the consoling power of nature experienced by the characters when they are with the natural setting in the novel *The Tree of Man* written by Patrick White. The study is an eco psychological re-reading of the text which will allow readers to witness how the environment becomes an inevitable part of human life that reflects the interconnectedness of all that the nature has created. The escape to nature has another appeal besides its beauty and tranquillity. It is freely available to the poor as well as to the rich. Ecological interactions touch an individual's physical, spiritual, emotional and psychological facets of life. Eco psychology is a modern social and intellectual movement aimed at recognizing and harmonizing the relationship between people and the Earth. The emerging field of eco psychology is showing how our human psyches are closely bound to the elemental earth.

Earth centred faiths strives to honour the strength of nature's consoling power. This eco psychological study shows how the text demonstrates the character's harmonious and balanced eco human bonding. It shows how far identities of characters are shaped by the surroundings in which they live. The study describes how the ecological lifestyle is an encompassing transformation that touches every facets of an individual's life. The experiences encountered by the characters in the novel shows how the experiences in life with the natural environment move them towards a greater appreciation and concern for the natural world. Thus the paper studies *The Tree of Man* as an ecological writing with a literature of hope.

In the novel, the characters sufferings in life get consoled as they get along with nature.

When they remain in both wild and domesticated environments, most often in places of natural beauty, there are revelatory experiences awakening their wisdom and modesty. Experiences with the destructive sides of nature can test the commitment of ecological followers to provide a powerful reminder that a turn of earth is not peace, safety, or limitless abundance. In its natural cycles and changing ecology, the environment offers great stability, but this constancy is not fully chaos-free. Biophilia, the love of nature and living things, is an essential part of the human condition. Those who spend extensive time in the environment observe to respect the extreme spontaneity of nature.

Patrick White's novel evokes a diversity of landscapes that often enter into the texture of the novel's narrative. He is quite a few steps ahead of the other contemporary writers. His works reveal the depth of his understanding of Australia as a region and its atmosphere. White considers it not only as a land of mystical values but also as a separate entity in human life. The depth in which he depicts the landscape of the Australian nation, reality encounters with nature thereby resulting in idiosyncratic revelations makes his works stand apart from other writers. Patrick White's *The Tree of Man* evokes a diversity of landscapes that often enter into the texture of the novel's narrative.

People are less stressed when they are with nature. Eco criticism helps us to realize that all living organisms are connected when we step into nature. Nature gives comfort to all troubles. The word '

tree ' in this novel's title stands for the search for growth of Stan, for the unbounded life. Stan was a person who loves to be with nature. The novel begins with the description of two big trees as:

A cart drove between the two big stringy barks and stopped. These were the dominant trees in that part of the bush, rising above the involved scrub with the simplicity of true grandeur (1)

The novel is a beautiful evocative description of the nature. Patrick White has paid a lot of attention to the nature that surrounds his protagonist Stan Parker. "He smelled the smell of green wood. The name of this man was Stan Parker."(5 White) It is a suburban drama that tells a story of the lives and fortunes of the Parker family over many decades. Stan is a son of blacksmith and an educated mother. Stan's mother expects him to be a teacher or a preacher. After the death of the parents of Stan Parker, he decided to begin a new life. Stan had no intention of remaining in the confining atmosphere of the Australian bush town where he grew up. "At Willow Creek, God bent the trees till they streamed in the wind like beards. In the streets of towns the open windows, on the dusty roads the rooted trees, filled him with the melancholy longing for permanence."(13)

He leaves his hometown and travels to an unsettled area outside Sydney, where he has inherited some property. He manages to makes out a house in the woods and starts farming. Stan had come to the woods in search of peace. "Stan Parker began to tear the bush apart. His first tree fell through the white silence with a valley of leaves...Many days passed in this way, the man clearing his land...Seen through the trees; it was a plain but honest house that the man had built."(17)

White's heroes suffer from alienation when they are in the midst of human society. Stan loved living in the woods devoid of all the rush of the busy world. He wanted a peaceful life in the calm and soothing nature. Stan is a lonely man whose most outstanding characteristic is his quality of being silent. He loved to be part of nature and wished to settle his life there. Many days passed in this way, Stan clearing his land. At last he built his house amongst the woods. "Seen through the trees, it was a plain but honest house that the man has built."(17)

One day Stan brought with him a woman. Her name was Amy Fibbens. Stan's union with

Amy Fibbens played a key role in shaping his goal and his efforts to achieve it. When they came to the place where Stan's house stood, they were on the outskirts of the town, where they could smell sheep, and of water drying in a mud hole. The place was home to incredible scenery and delicate ecosystems. Stan's cart jolts through the windy countryside "The girl lazily smiled at the landscape, holding her hat."(25) It was a long ride through the bush road. The travel through the woods consoled her ill thoughts.

The girl sat with her eyes on the road. She was not concerned, as at odd moments, her husband was afraid she might be. Because in her complete ignorance of life, as it is lived and the complete poverty of the life she had lived, she was not sure but that might have to submit thus, interminably bolt upright in a cart. Life was perhaps a distances of stones and sun and wind, sand coloured and monotonous."(26)

Amy always had a feeling that Stan remains distanced from her. Her only relief is observed from the surrounding she lives. This consoling power of nature has brought Amy Parker to live in the midst of the beauty of nature. Amy Parker had grown greedy for love. She had not succeeded in keeping her husband with her all the time. She had promised herself in moments of indulgence that she would achieve this at some future date. But she fails every time. Amy's only relief was the moments she had with the nature. Amy loved animals and enjoyed planting trees. "She should plant the white rose,

where the slope of the land was still restless from the jagged stumps of felled trees."(28) The nature which surrounded her spoke to her in its silence from her consoling depths.

"She walked slowly on, taking care of herself, and the harsh blue of her wooden jacket flickered through the evening colours of the garden, the colour of moss, almost of foreboding, and her skirt in passing stirred up an intolerable scent of rosemary and thyme that lingered after she had gone."(57)

The Parkers continued their life. When Stan leaves the house into the woods he can still hear the voice of Amy when he was alone in nature. To discover what life actually is, the more humble Stan Parker turns to Nature. Stan's greatest strength is his endurance. His mind can withstand pain and torture to the degree that it can help him achieve his goal. Other people came to live in that place after few years and there is a rose bush now , growing against the veranda , a white rose , of which Amy had thought and spoken to Stan , and which he had brought to her from the town.

The major event that took place was a great flood, which fortunately did not destroy their farm. The still air became more charged the closer they got to the centre of the storm, the sky darker. The storm continued most of the days: "The whole earth was in motion and streaming trees, and was in danger of being carried with it."(47)

The constant rain that swells into the flood of Wallonia, causes trouble to people's lives, and

Stan is brought to the point that he understands how weak man is. He joins other volunteers and helps rescue settlers stranded by the flood.

The great trees had broken off, two or three fell". "He remembered the face of his mother before her burial, when the skull disclosed what the eyes had always hidden; some fear that the solidity of things around her was not assured. But on the dissolved world of flowing water, under the drifting trees, it was obvious that solidity is not. (73)

Stan learns to humble himself from his surroundings and to embrace continuous changes as the only solidity. Two children are born to the Parkers, a daughter, Thelma, and a son, Ray. Later, during a raging bushfire, Stan rescues Madeleine from the burning manor house. World War I begins soon after the great fire, and Stan enlists in the army. After Stan returns from the battlefields of France, he once more works his farm while his wife carries out her domestic duties faithfully and his children grow into adults. "One was born. One lived". (104) Stan felt that staying isolated in the nature is the only way to consolation. It reflects one's self confidence. He admires the land which gives shape to his life. Also he is also looking for a sense that lies beyond the visible environment. The solitary life in nature helps to develop internally from which a person eventually must reach the innermost core of his own being. "Society, as such, fills him with discomfort and it has always remained an "unrealized ambition". (186) Stan feels the land is an indomitable power, bringing misery, suffering and desolation. These ecstatic experiences faced with the nature makes a person stronger.

Works Cited

1. White, Patrick. *The Tree of Man*. London: Vintage, 1994. Print.

IJIREEICE

ISSN (Online) 2278-1021
ISSN (Print) 2319-5940

International Journal of Innovative Research in
Electrical, Electronics, Instrumentation and Control Engineering
NCIET- 2020
National Conference on Innovations in Engineering & Technology
Govt., Polytechnic College, Palakkad, Kerala
Vol. 8, Special Issue 1, February 2020

Evaluation of Current Design Practices for Horizontal Curves on Rural Highways Based on Vehicle Stability and Safety

Y K Remya[1], Anitha Jacob[2], E A Subaida[3]

Assistant Professor, Department of Civil Engineering, SCMS College of Engineering and Technology, Karukutty, India[1]

Lecturer, Department of Civil Engineering, Govt. Polytechnic College, Chelakkara, Thrissur, India[2]

Associate Professor, Department of Civil Engineering, Govt Engineering College, Thrissur, India[3]

Abstract: All over the world India bangs the top most position in deaths caused by road crashes. Over 1 lakh people are killed or seriously injured in road crashes in India every year, that is more than the number of people killed in all our wars put together. Sixteen children die on Indian rroads daily and there is at least one death every four minutes. Majority of the crashes are found to take place on rural highways. Rural highways are characterized by a low traffic volume and hence, speed of the vehicles is mainly controlled by the geometry. The topological conditions of India have resulted in very complex curves which include combination of horizontal curve and steep gradients up or down. In such environment, the drivers tend to choose the speeds that they perceive to be comfortable to them based on their perception of the criticality of the road geometrics ahead. Any unexpected road feature in the highway may surprise the drivers and may result in erroneous driving manoeuvres, which in turn, may end up in road crashes. As highways are meant for high speed travel, the impact of any collision that takes place will be grievous or fatal. Hence, the highways have to be designed such that their geometry directs the drivers to choose the operating speed which is in harmony with the environment.

A large number of studies are done to evaluate the effect of geometry on operating speed of rural curves. But only a few researches are done to assess the effect of geometry on the stability of vehicles. Skidding and rollover crashes are increasing dramatically, the first being more common in small vehicles like cars and the latter being more common in heavy commercial vehicles like trucks. The availability of sufficient lateral friction to counteract centrifugal force experienced by a vehicle on curve is least studied, especially in India. The values of lateral friction adopted for design of horizontal curves were developed eighty years ago by Barnett 1936; Moyer and Berry 1940. Since then, vehicle fleet has changed completely and hence the demand for lateral friction may also have changed. But the point mass equation widely used for design of horizontal curve relies on lateral friction values developed by them. Also, the equation ignores the effect of vehicular characteristics or complexity of curve geometry. So, studies focusing on revision of geometric design criteria of horizontal curves based on vehicle stability and assessment of existing margin of safety or in other words, a quantitative assessment of risk involved affecting the stability of vehicles is very important. In this paper an effort has been made to identify the gaps in current design practices and to exhibit current status of study in the field of vehicle stability on rural highways.

Keywords: Skidding, Friction, Vehicle Stability, Rollover.

I. INTRODUCTION

When a vehicle travels along a horizontal circular curve, it experiences centrifugal force outward the centre of the horizontal curve. This centrifugal force is inversely proportional to the radius of horizontal curve. Vehicle stability is achieved by the resistive forces that resist the centrifugal force. These forces include frictional interaction between the tires and pavement, and a component of the vehicle weight that acts parallel to the road surface. The frictional interaction between the tires and pavement depends on road surface side-friction factor, which in turn depends on many other factors, including road surface condition, weather and climatic condition, tire condition, and vehicle kinematics. The component of the vehicle weight that acts parallel to the road surface depends on the side slope of the highway, which is usually termed as superelevation. This approach is usually referred to as the point-mass (PM) model, which is adopted by North American design guides due to its simplicity.

Based on the point-mass model, when a vehicle travels along a vertical curve, there is obviously no centrifugal force, and consequently no potential risk for skidding or rollover. However, for 3D(combined) alignments, where a horizontal curve is superimposed by a vertical alignment, the vertical alignment affects the available side friction. For 3D alignments, traditional design guides (AASHTO 2001; TAC 1999) calculate the minimum radius assuming a side friction on a horizontal plane using the point-mass model, thus ignoring the effect of vertical alignment. This approach simplifies cornering dynamics by reducing the vehicle into a point mass travelling on a 2D horizontal alignment.

Salinity reduction in well water using zeolite

M R Sruthy[1], M Akhila and Neena Rose Davis

Department of Civil Engineering, SCMS School of Engineering and Technology, Ernakulam, Kerala, India

[1]E-mail: sruthy@scmsgroup.org

Abstract. Saline water intrusion is one of the global issues, which increases the demand for freshwater around the coastal region. The saline content in drinking water makes so many health impacts on human beings. There are many new technologies available for reducing salinity such as desalination, membrane technologies, reverse osmosis, etc. But these are expensive too. There is a need for cost-effective treatment which is suitable for domestic purpose in coastal regions. In this paper, a new technique is introduced which reduces the saline content in groundwater by installing this barrier device in wells of coastal regions. A non-woven Geo textile along with natural zeolite is used as a filter cum adsorption unit. Tests results show a decrease in electrical conductivity and total dissolved solids with an increase in filter thickness for all selected salt concentrations irrespective of the adsorbent materials used viz., natural zeolite and thermally activated natural zeolite. This indicated a reduction in chloride ions as the only salt added to the water samples tested was commercial salt. Authors suggest that a thermally activated zeolite filter could be a possible cost-effective, efficient and easy solution for increasing saline water intrusion issues in coastal drinking water wells.

1. Introduction

Saltwater intrusion, which is the induced flow of saline or brackish water into freshwater, is an ever-increasing problem in coastal areas. Seawater intrusion is often regarded as the only factor causing saltwater contamination. But, there are seven other causes of salinity in groundwater like tidal and storm surges, pollution from agricultural land, etc [1].Once saltwater intrusion occurs, the changes in the aquifer may be permanent or may take many years to recover.

Saline water intrusion impacts are associated primarily with losses of freshwater resources and contamination of water supply wells, and only a few studies consider adverse ecological impacts directly linked to saline water intrusion. Environmental degradation arising from this is commonly linked to the application of high salinity groundwater in agriculture, resulting in modified soil chemistry and reduced soil fertility [2]. While the direct and indirect intrusion of salinity in fresh groundwater affects human well-being, its serious implications on population health must be clearly understood. Owing to the use of saltwater, numerous diseases including skin ailments, hair fall, diarrhoea, gastric diseases, and high blood pressure are suffered.

A lot of techniques have been used to manage/control salt/seawater intrusion and protect groundwater resources. The principle is basically to reduce the volume of saltwater intrusion and increase the volume of freshwater. Mahesha [3] and Rastogi et al. [4] combined the methods of injection of freshwater and extraction of saline water to increase the volume of freshwater and to reduce the volume of saltwater pose effective but the setback is the cost factor involved in the construction and maintenance of the wells. Several of these methods are costly and some might not be

Liquefaction resistance improvement of silty sands using cyclic preloading

Akhila M[1,3], Rangaswamy K[2] and Sankar N[2]

[1]Department of Civil Engineering, SCMS School of Engineering and Technology, Ernakulam, Kerala, India
[2]Department of Civil Engineering, NIT Calicut, Kerala, India

[3]E-mail: akhilam@scmsgroup.org

Abstract. Liquefaction induced damages are plenty and cause various levels of destruction to civil engineering infrastructure. It is possible to prevent liquefaction-induced hazards by understanding the mechanism and adopting some improvement techniques or design the structure to resist the soil liquefaction. In the present study, the influence of cyclic preloading on the liquefaction resistance of sand-silt mixtures is analyzed by conducting undrained cyclic triaxial tests on the cylindrical samples reconstituted at medium dense conditions (D_r = 50%). All samples were tested at an effective confining pressure of 100 kPa by varying the cyclic stress ratios (CSR) in the range of 0.127 to 0.178 using a sinusoidal waveform of frequency 1 Hz. The results are presented in the forms of the pore pressure build-up, axial strain variation and liquefaction resistance curves. Test results indicate that the liquefaction resistance of silty sands is increased substantially with the application of preload under drained conditions.

1. Introduction

Liquefaction induced damages are plenty and cause various levels of destruction to civil engineering infrastructure. It is possible to prevent liquefaction-induced hazards by understanding the mechanism and adopting some improvement techniques or design the structure to resist the soil liquefaction. The first possibility is to avoid the construction on liquefiable soil deposits as far as possible. However, it is mandatory to utilize the available land for the various infrastructure developments due to scarcity in the availability of land even it does not satisfy the required properties. Hence, the second option is to make the structure resistant to liquefaction by adopting deep foundations. Nevertheless, the deep pile foundations may not prevent liquefaction damages in all cases. Piles are causing to deflect in liquefaction susceptibility zones. Hence, the third option is liquefaction mitigation which involves improving the strength, density, and drainage characteristics of the soil. The selection of the most appropriate ground improvement method for a particular application could depend on many factors including the type of soil, level, and magnitude of improvement to be attained, required depth and extent of the area to be covered. This paper presents an experimental study regarding the applicability of preloading for the improvement of liquefaction resistance.

2. Literature review

Preloading of the soils occurs naturally (for eg., erosion, the flow of groundwater, etc) or artificially (purposeful preloading to improve the soil properties, demolition of structures, etc). A few researchers have analyzed the liquefaction resistance of preloaded soils. The details are given in Table 1.

Materials Today: Proceedings 42 (2021) 1100–1105

Contents lists available at ScienceDirect

Materials Today: Proceedings

journal homepage: www.elsevier.com/locate/matpr

A review on the use of ferrocement with stainless steel mesh as a rehabilitation technique

Juby Mariam Boban, Anjana Susan John*

Department of Civil Engineering, SCMS School of Engineering and Technology, Kerala, India

ARTICLE INFO

Article history:
Received 29 September 2020
Received in revised form 6 December 2020
Accepted 10 December 2020
Available online 3 February 2021

Keywords:
Rectangular columns
Preload
Stainless steel
Ferrocement confinement
Rehabilitation
Ultimate load

ABSTRACT

One of the major issue faced by the construction industry is the degradation of structures due to different loads acting on the structure. So retrofitting and rehabilitation has become quite inevitable and it can help in regaining the original strength of the structure. Use of ferrocement is an effective method and it is used in developed countries as it is considerably cheap and materials of construction are easily available. Ferrocement is a system of construction using reinforced mortar or plaster applied over an armature of metal mesh, woven expanded-metal or metal-fibers and closely spaced thin steel rods such as rebar. The skill required is of low level and it has superior strength properties as compared to conventional reinforced concrete. The main drawback of ferrocement is corrosion. Thus to avoid corrosion stainless steel jacketing is employed for rehabilitation within the study that opens the scope for a new jacketing methodology.

Selection and peer-review under responsibility of the scientific committee of the Second International Conference on Recent Advances in Materials and Manufacturing 2020.

1. Introduction

Concrete is the most popular construction material which is made of cement, aggregate and water. Water is acting as the bonding agent between the component. On adding water, the concrete is in a plastic state and acquires strength with time. Portland cement is the ordinarily used type of cement for production of concrete. Concrete is used in the construction of the major structural elements like foundations, columns, beams, slabs and other load bearing components. The use of traditional construction materials such as steel and concrete showed signs of deterioration due to prolonged action of loads which results in degradation of overall strength of the structure which makes it futile. This degradation is a result of poor construction techniques, flaws in designing process or may be due to poor updating of the methods specified in design codes. Proper maintenance is a partial solution. So is a necessity of an effective rehabilitation technique which will improve the life expectancy of the structure. Earlier studies focused on steel meshes which is prone to corrosion. My study focuses on a non corrosive technology for rehabilitation. The scope of stainless steel as a jacketing method is not studied formerly.

In most of the developed countries, the development trade has almost reached saturation. So there is an increasing demand to ameliorate and strengthen the existing structure instead of demolishing. The damages are mainly due to the environment degradation, design inadequacies, poor construction practices, irregular maintenance, requirement of revision of codes in practice, increase in the loads and seismic conditions etc. Rehabilitation is one of the practical solution for such structural collapse and it can be done effectively by strengthening the load bearing components or by strengthening the vital components of the building which results in the failure of the building. Therefore, rehabilitation and upgrading of degraded structure has become one among the foremost vital challenges in development industry. In several cases, the whole demolition of the existing structure is not an economical answer as it becomes an exaggerated money burden. So upgrading or repairing the structure is an effective practical approach. Column is the major compression load bearing component member and the failure of which results in the failure of the whole building. During earthquakes, columns are likely to undergo brittle failure. So the ductility of columns has to be improved to prevent the inelastic deformation occurred during earthquakes. Whereas repair and rehabilitation using ferrocement enhance the strength and ductility of the column. Proper selection of the strengthening material is inevitable to enhance the properties of the column.

* Corresponding author.
E-mail address: anjanajohn@scmsgroup.org (A. Susan John).

https://doi.org/10.1016/j.matpr.2020.12.490
2214-7853/
Selection and peer-review under responsibility of the scientific committee of the Second International Conference on Recent Advances in Materials and Manufacturing 2020.

Effect of Plasticity of Fines on Properties of Uniformly Graded Fine Sand

M. Akhila, K. Rangaswamy, N. Sankar, and M. R. Sruthy

1 Introduction

Even though researchers separate soils based on particle size as sand, silt and clay, in the field, soil always exists as a combination of all these. There are many studies concentrating on the effect of fines on the shear characteristics of sand [1–3] and liquefaction [4–7] but only a few studies have considered the other properties.

Yang and Wei [8] have analysed the change in critical state friction angle for Fujian and Toyoura sands. For clean sand without fines, the critical state friction angle tends to decrease with increasing roundness of sand particles. When those sands were tested with fines (round shape), the critical state friction angle of the mixture tends to decrease with an increase in fines content. But for fines with an angular shape, the critical state friction angle tends to increase with fines content. Phan et al. [9] have conducted one-dimensional consolidation tests on sand–silt mixtures (with low-plastic fines at a constant void ratio and constant relative density) and indicated that the behaviour of the mixtures were similar to those of loose sand. The effect of fines on void ratios was studied by Cubrinovski and Ishihara [10]. The authors reported that the void ratio initially decreases as the fines content increases from 0–20% and above 40% fines, the maximum and minimum void ratios were seen to increase steadily.

It is clear from the literature that the studies on the effect of plasticity of fines on the properties of sand are limited. Hence, the present study is focused on the effect of the amount of fines and the type of fines (or plasticity index of fines) on various properties of sand like specific gravity, limiting void ratios, grain size characteristics, angle of internal friction and compression index.

M. Akhila (✉) · M. R. Sruthy
SCMS School of Engineering and Technology, Ernakulam, Kerala, India

K. Rangaswamy · N. Sankar
NIT Calicut, Kozhikode, Kerala, India

C. N. V. Satyanarayana Reddy et al. (eds.), *Ground Characterization and Foundations*,
Lecture Notes in Civil Engineering 167,
https://doi.org/10.1007/978-981-16-3383-6_1

Modernizing Traditional Methods of Farming using Farming Robot

Ashby Babu[a], Samal Muhammad[b], Arjun Subramanian[a], *Sreeja Rajesh[c], Vinod P[d]

[a]*Research Scholar, SCMS School of Engineering & Technology, Ernakulam, Kerala, India*
[b]*Trainee, Infosys Ltd., Ernakulam, Kerala, India*
[c]*Assistant Professor, SCMS School of Engineering & Technology, Ernakulam, Kerala, India*
[d]*Professor, CUSAT, Kochi, Kerala, India*

ABSTRACT

This paper pertains to the study of a prototype which modernizes the agricultural sector. It has the ability to perform basic operations such as irrigation activity and monitoring of plants frequently without much manual labor. In addition to the above-mentioned functionalities, the system is trained for detecting diseases in plants. Agriculture is an area of prime importance in the existence of humanity. It is a process of cultivating land and plants to provide food, fiber, medicines and other products to enhance the quality of life. It is considered to be the main pivoting point in the rise of our civilization. In the proposed system ROFAR, detection of plant disease is achieved with the help of image processing and machine learning methods. Prompt and accurate detection of plant diseases is crucial for the quality and yield of crops. Advanced diagnosis and intervention can lower the cost of plant diseases and trim down the use of unnecessary pesticides. Images of leaves of different plant species were gathered and feature extraction was performed. As a result, the system was able to classify the plants based on its ailments accurately. The ROFAR gathers the images of the plants for disease detection from the field and were given as input to Convolution Neural Network (CNN) which then classifies the images as healthy or infected. The proposed system ROFAR undergoes a training phase and a testing phase. The system is trained by providing various samples of the normal and diseased plants. On completion of training phase, the system can identify any new images of plants as healthy, late blight, viral or bacterial. The system also facilitates the moisture detection in the soil. With these functionalities, crops with better quality and yield can be obtained from the field.

Keywords: ROFAR, Convolution Neural Network (CNN), Training phase, Testing phase, moisture detection, late blight, bacterial, Feature extraction.

1. Introduction

One of the most promising and upcoming technologies that has the capacity to boost almost all the sectors of the economy, from medical to space sectors is Robotics. However, the sector that is constantly lagging is agriculture. It's due to the fact that many farmers are being used to heavy equipment, tools and conventional agricultural strategies. Although the application of robotics in this sector is slow, it's persistent.

The utilization of technologies that are linked with robotics and automation, can provide important values to both farmers as well as the agricultural sector [1]. These automated bots are being used for conventional applications which includes plant classification, fruit picking, seeding, spraying, etc. Machine-driven agricultural operations introduce many advances to the field improving the overall productivity and efficiency. Automation provides countless perks to farmers or landowners which makes the job performed in a uniform method, with less expense and higher accurately. The processor located at the centre of the Raspberry Pi framework is a Broadcom BCM2835 framework on-chip (SoC) mixed media processor. This indicates by means of a ways most of the framework's segments, consisting of its illustrations and focal preparing units beside the correspondence's equipment and sound, constructed onto that solitary segment beneath the memory chip of 256MB situated at the centre point of the board. The fact that makes BCM2835 different from the processor determined for your workplace or PC is not simply its SoC structure. In addition, it makes use of an Industry Standard Architecture (ISA) which is known as ARM [2]. The significance of water splashing is one of the principal applications performed. Water transports vital supplements within the plant. The

supplements are extracted from the earth and used by the plant. Inadequate water in the plant cells causes the plants to stop growing, so water allows the plant to stand upright. The water carries the disintegrated sugar and various necessary supplements through the plant. So, without the correct equalization of water, the plant is not exclusively undernourished, however it is too physically weak and can't bolster its very own load. Various sorts of plants require various measures of water [3]. With open air plants, we can't manage the plants getting an excess of water if the area gets a great deal of downpour, so we have to ensure that the dirt has the correct seepage, since large amounts of water will influence plant development the same amount as excessively little. Video observing of the plants is additionally of most extreme significance. The programmed plant checking framework had a huge enthusiasm because of the promising applications in rising innovation. Although, this strategy is used to enhance the execution of existing methods or to make and structure new procedures for the growth of plants. The plant checking framework is mainly used for watering the plants and to transmit a couple of parameters for growth of plants. Plant illness recognition is the fundamental utilization of the pack. Plant malady, a weakness in the plant's normal condition that hinders or regulates its vital capabilities. All kinds of flora, wild and evolved alike can suffer from disease [4]. The percentage of plant infections varies from season to season, natural conditions, contact with the pathogen and the crops and assortments developed. Some assortments of the plants are prone to disease outbreaks, while others progressively resistant them. Fossil proof demonstrates that plants were influenced by illness 250 million years back. Loss of yields from plant maladies may likewise result in appetite and starvation, particularly in less-created nations where access to ailment control techniques is restricted and yearly misfortunes of 30 to 50 percent are normal for real harvests. In certain years, misfortunes are a lot more prominent, creating calamitous outcomes for the individuals who rely upon the yield for sustenance. Real ailment flare-ups among sustenance crops have prompted starvations and mass movements since forever [5].

The proposed automated system captures the images of the plants and has a detecting mechanism for classifying the plant as diseased or healthy. A real-time video monitoring system incorporated in the proposed system facilitates the user to be aware of the conditions in the field. In addition to these features humidity of the soil is measured and decision on spraying water to the plants is taken care.

The remainder of the paper is structured as follows: Section 2 deals with Literature Survey. Section 3 describes the Hardware and Software Components used to build the prototype. Section 4 illustrates the proposed model, working principle and the implementation. Section 5 deals with the experimental analysis and the result. Section 6 describes the conclusion. Section 7 describes the future scope of the project. Lastly, Section 8 lists all the references used in this paper.

Nomenclature

ABC Atanasoff Berry Computer
AI Artificial Intelligence
ANN Artificial Neural network
ARM Acorn/Advanced RISC Machine
BCM Body Control Module
CNN Convolution Neural Network
DNN Dynamic Neural Network
GNU GNU's Not Unix
GPIO General Purpose Input/output
GUI Graphical User Interface
IDE Integrated Development Environment
IDLE Integrated Development and Learning Environment
IoT internet of Things
ISA Industry Standard Architecture
ML Machine Learning
(N;P;K) (Nitrogen; Phosphorus; Potassium)
PC Personal Computer
pH Potential of Hydrogen
RFB Remote Frame Buffer convention

SoC System on a Chip VNC Virtual Networking Computing

2. Literature Survey

2.1. Algorithm for Line Follower Robots to Follow Critical Paths with Minimum Number of Sensors

The main challenge faced in the area of robotics is that going along a specified path [6]. Either the path could be designed by the user or it could sense a particular color and move along that path. When specified by the user's intermediate counters for stopping and turning could be initially kept precise. However, each color has its own threshold, and the robot senses its movement with respect to the color. This paper discusses line follower robots, their configuration and inculcates a concept for the robot to move along curves, junctions and 90-degree bends. Therefore, the line follower robots are autonomous, having the ability to follow and detect a line ensuring the base to an efficient system. The project employs Arduino Uno as the main circuit board for the robot and four sensors for following the path. The robot uses 4 IR sensors S_{LL}, S_L, S_R and S_{RR} arranged on a straight path for detecting the line as shown in the Fig. 1. The sensors S_{LL} and S_{RR} are used to perform 90-degree rotation on left of right respectively.

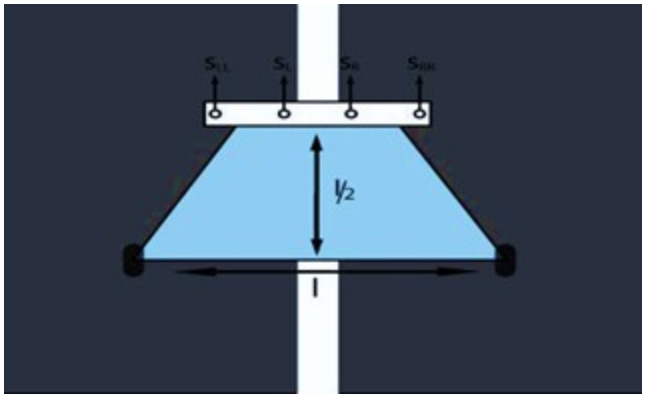

Fig. 1- Robot sensor diagram

If any of the sensors deviate from its original position, then the robot corrects itself by moving along right or left. If any of the two sensors come on the white line, then a 90-degree turn is done according to the algorithm. Therefore, based on two main algorithms it can follow the path given to it. When implemented the robot also must account for obstacles in its path and proper halts in the junctions to do the specific jobs that it aims to do. The paper resembles such an algorithm for following the path with precision and proper configuration of the sensors. A prototype built by J S Tan et. al. known as Jackbot Mark1 is a cheaper, light weight and small robot that has an ability to move and carry load incorporating obstacle detection, line following algorithms [7]. Mehran Pakdaman et. al. discussed various technical problems that could arise in any line following robot [8]. The challenges involved while navigating in a constrained environment like greenhouse and polytunnels are addressed using an autonomous row following robot [9,10].

2.2. Design and Implementation of Semi-Autonomous Anti-Pesticide Spraying and Insect Repellent Mobile Robot for Agricultural Applications

The authors discuss on the application of robots in agriculture. It focuses on designing a robot called "x-bot" which is an insect repellent robot and a pesticide sprayer [11]. The main problem with the manual spraying of pesticides is the over spraying causing harm to both plants and humans. Thus, the robot is designed to overcome this problem. An additional unit of insect repelling mechanism with the help of a sonar is also built and attached to the robot. The robot body is Lynx Motion Rover Kit with 3D

printed acrylic chassis and four dc motors are used to drive the robot. Arduino Mega Microcontroller is the control unit with diaphragm pump to spray pesticide and solar panel attached buzzer to repel insects. Proportional Integrative Derivative algorithm is employed to control the robot and as the robot reaches each of its spots, pesticide is sprayed at a precise amount. Alongside the insect repellent is also done. In addition, the ultrasonic sensors are calibrated by the neural networks.

2.3. Design of automatic nutrition supply system using IoT technique in modern cities

Today, the main problem faced by Terrace Gardening is the lack of time for the planters to look after the garden on a regular basis [12]. The one available solution is by employing smart farming which modernizes the current conventional methods of farming in modern cities. Modernizing includes automation of almost every process in the area of farming. This paper discusses the automated system by applying the concept of IoT. The primary objective of this study is to provide the plants with the necessary nutrients, such as potassium, phosphorus, nitrogen and calcium, which is computed from the data provided by the sensors. The pH value of the soil is taken by the pH sensor attached to the Raspberry Pi. The pH value is processed along with the Humidity sensor. Value of the humidity sensor is considered on the basis that when Humidity increases the chance of plants to get caught by disease is high and the rate of growth of plants will be low and vice versa. Therefore, based on these values and calculations the nutrients are supplied to plants. The authors developed an automatic nutrient supply system which is capable of passing nutrients mixed with water automatically to the plants as required thus reducing the human labor to a great extent. Measurement of the pH of the solution provides data about the nutrient's availability in the soil. The quantity of fertilizer is supplied according to the requirement of the crops. This system could help in the better use of fertilizer and to enhance the quality of soil. The limitations to this system are, absence of weed detection and control mechanism, seed plantation and the system is immobile in nature. Sajjad Yaghoubi et. al. suggested an autonomous robot that aims to reduce manpower and to improve the quality and productivity of farming [13].

2.4. Real-time Video Monitoring and Micro-Parameters measurement using Sensor Networks for Efficient Farming

One of the main challenges faced in the area of farming is that there is no system that monitors the field which gives the advantage to the farmer to monitor the farm on a real-time basis [14]. The solution to this problem is to design a Robot that can monitor the system on a real-time basis which is equipped with a camera along with a Robotic arm and sensors that helps to monitor the plant growth. The robotic arm is used to measure and manage agricultural parameters. The robotic design in this study is composed of sensor, control, camera, planning subsystem and a system comprising an online image and video transmitter. The constituent of potassium, phosphorus and nitrogen present in the soil is measured in order to depict the amount of fertilizer required by the soil. This mechanism also aids in managing the content measurement while preparing the fertilizer. The primary goal of this design is the reduction in the number of nodes required for the conventional measurement schemes. There are mainly two blocks. One block indicates the transmitter, which is actually, the Robot and the other block depicts the receiver. The System is employed to design, develop and optimize a feasible solution to agricultural control and monitoring. The proposed system utilizes sensors for Micro parameter measurement (K, P, N), Humidity measurement, Soil moisture, Motion detection, temperature detection, Soil PH for maintaining agricultural environment. It also includes Agricultural Parameters measurement and Real-time Video Monitoring using Sensor Networks for Precision Agriculture. After the proper measurement of K, P, N content from soil it will be easy to figure out the fertilizer combinations. On implantation, it is found that System results in the designing, development and optimization of a feasible solution for application to agricultural control and monitoring. The limitations to this system are, absence of weed detection and control mechanism, seed plantation and the inability to supply nutrients and water to the plants.

2.5. Design of automatic nutrition supply system using IoT technique in modern cities

The most prominent troubles faced in farming is that much vegetation are laid low with sickness. Every 12 months illness of the plant, fungal and viruses' attacks result in crop losses as much as 30% of the overall production [15]. The plant disease control mechanism relies upon speedy, correct detection and identification of the diseases. The paper discusses correctly figuring out the

disease with the help of an artificial neural network. The different image processing performed on the input image are image enhancement and image segmentation. The Fig 2 shows the block diagram of plant disease detection and depicts the various texture feature values that are computed from the processed image. The classification of text image is performed at last by giving the extracted feature values as an input to the pertained artificial neural network (ANN). Finally, the predicted result (disease) is sent to the person.

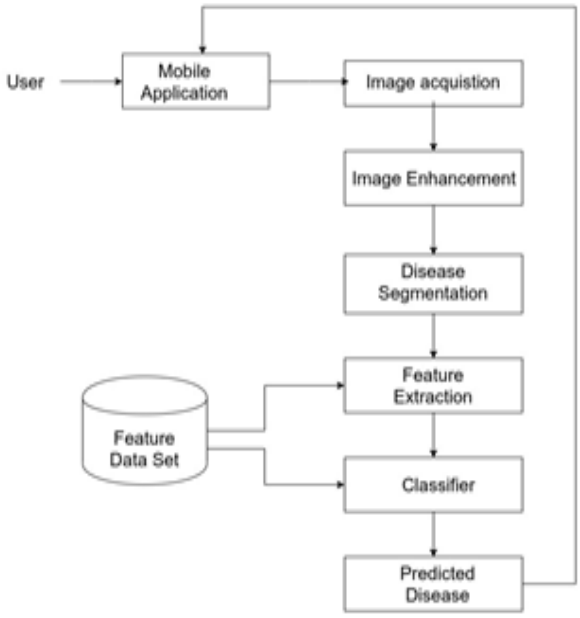

Fig. 2: Block diagram of plant disease detection

The network used is a feed forward neural network of two layers with one hidden layer, in which number of neurons for hidden layer is 10. The method specified in the system can be used to design a plant disease detector for farmers for the early detection of plant disease infection and providing a cure remotely.

2.6. Design and development of Automatic weed detection and smart herbicide sprayer robot

Traditional method of destroying the weeds in a crop plantation is achieved by spraying herbicides throughout the plantation [16]. This has a bad effect on food crops and yield. This paper discusses the image processing algorithm which captures the images of plantations and the herbicides sprayed only on the weeds on identifying the weeds from the image. By this method, the wastage of herbicides can be reduced to a great extent thus making the weed control system smarter. The color images will be converted to binary images and the green parts of the image are extracted. Total amount of white pixels is found out, if it is above threshold then that region is weed. In this arrangement, a container filled with herbicide is fitted with water pump motors which is attached to the spray nozzles. In this experiment Ragi plants (narrow) are taken as the plantation crops and any other plants as weeds (broad leaves). In the absence of plants on the region of interest, the processed image will encounter only black pixels with few small stray groups of white pixels. On identifying narrow leaves, the number of white pixels could be greater than case 1 but less than threshold. If there are broad leaves the count of white pixels will be greater than threshold. Herbicide will be sprayed on this region since its weed. This approach is dependent on the quality of the lighting conditions required for capturing images which is one of the disadvantages faced by smart weed control robots. By incorporating targeted spraying on the weeds, wastage of herbicides can be reduced to a great extent [17-21].

3. Hardware and Software Components

3.1. Algorithm for Line Follower Robots to Follow Critical Paths with Minimum Number of Sensors

The Raspberry Pi, (Fig. 3) is intended to run a working framework called GNU/Linux—from this point forward alluded to just as Linux. In contrast to Windows or OS X, Linux is open source: it's convenient to download the source code for the whole working framework and add whatever improvements you want. Nothing is hidden, and all progressions are made in full perspective on people in general. This open source improvement attribute has enabled Linux to be immediately transformed to keep running on the Raspberry Pi, a process known as porting. At the time of this composition, a few adaptations of Linux known as appropriations have been ported to the Raspberry Pi's BCM2835 chip, including Debian, Fedora Remix and Arch Linux. The different appropriations take into account various requirements, but still they all are open source.

Fig. 3: Raspberry Pi

Since its demonstration, Python has developed in ubiquity on the account of what is viewed as a reasonable and expressive grammar created with an importance on guaranteeing that code is meaningful. Python is an abnormal state language. This means Python code is written in generally prominent English, making the Pi with directions in a way that rushes to learn and simple to pursue. This is in checked difference to low-level accent, similar to constructing agent, which are nearer to how the PC "considers" yet practically inconceivable for a human to pursue without involvement. The abnormal state nature and clear language structure of Python makes it a gainful instrument for any individual who needs to figure out how to program. Another option is to make use of a coordinated improvement condition (IDE, for example, IDLE, which gives Python-explicit usefulness that is absent from a standard content manager, including punctuation checking, investigating offices and the capacity to run your program without leaving the supervisor. The VNC watcher is seen as the primary programming device utilized for the venture. At registration, Virtual Network Computing (VNC) is a graphical workspace that shares a framework which uses the Remote Frame Buffer (RFB) convention to remotely control another PC. It transmits the mouse and console occasions starting with one PC then onto the next, handing off the graphical screen refreshes back the other way, over a system [22]. It is stage free, there are customers and servers for some, GUI-based running frameworks and for Java. Meanwhile, several clients can interact with a VNC server. Common applications for this innovation include remote expert assistance and capturing work PC logs from home PC or vice versa. There are several versions of VNC that offer their own particular utility, For example, some efficient for Microsoft Windows or offering record exchange (not part of VNC legitimate), etc. Many are perfect (without their additional highlights) with VNC appropriate as in a watcher, as of one type can bind to a server of another. Others depend on the VNC code, but don't work well with standard VNC. In the typical strategy for an activity, a watcher interacts with a port on the server (default port: 5900). On the other hand, (depending on usage) a program can bind to the server (default port: 5800). Also, a server can interact with a watcher in "listen mode" on port 5500. The correct position of the listen mode is that the server site does not need to configure its firewall to allow access on port 5800 (or 5900), the obligation is the watcher, which is useful if the server site does not have PC capability and the watcher client is progressively competent.

The ROFAR system is shown in Fig. 4. The camera component is connected to one of the USB-A ports in the raspberry pi. For the dc motor connection, a L293D motor driver is used. For that import the time module and the GPIO pins. The output pin is comprised of Pin 22, 18 and 16. The enable pin of L293D is connected to the pin 22 of raspberry pi in order to enhance the

motor's running time. The motor is turned off when low. Motor 1 and Motor 2 are input pins. The IR sensors are powered by +5V pin to enable the movement of the kit. Next, utilizing the black wire, the ground pins are connected to the ground of IR sensor and motor driver module. With the help of the yellow wire, the output pins of the sensors both 1 and 2 are connected to the GPIO pins and 3 respectively. The motors are operated using four pins (AB, A, B). These four pins are connected from GPIO 14, 4, 17 and 18 respectively. The white and orange wire collectively are used to form the connection for a single motor. Such that, there are two pairs for two motors. The motor driver module L293D is used to which the two motors are connected and is powered using a power bank. We have to ensure that the ground of the Raspberry Pi is connected to that of the power bank, only then our connection will work. Rest of the part is done from the user's system.

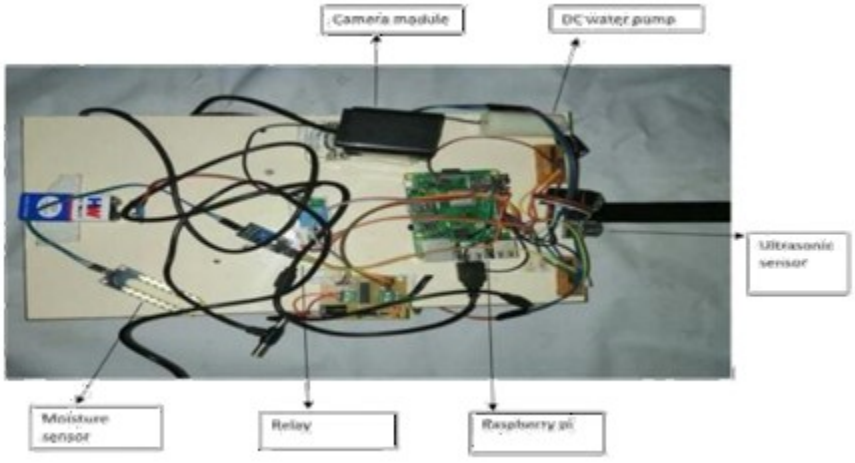

Fig. 4: ROFAR system

The raspberry pi is remotely accessed by the VNC viewer. There are mainly two python files accessed for the working one is named robot.py and the other named mail.py. The image of the plant is taken by the camera and is sent to the respective mail id set in the program.

4. Proposed Model

The proposed venture is completed for the most part by the raspberry pack and the plant leaf recognition by utilizing profound learning techniques in AI. Ongoing video observing is likewise included alongside the unit. The unit likewise showers the plant with water basically or by estimating the dampness of the dirt. At the point when the unit arrives near a plant it captures the images of the leaves and is sent back to a separate framework for malady recognition. The framework marks the plants with classes healthy(h), late-blight(l), viral(v) or bacterial(b). The robot then pursues a dark line utilizing the line following idea with the goal that it catches and plays out the splashing capacity up and down the way of the robot.

4.1. Line following Concept

The game plan of the plants is structured dependent on the way of the robot. The robot moves along the dark line taking the picture of the plants and in the meantime watering the plants. The robot distinguishes a line as a basic line and pursue basic line following calculation if both of its external sensors are on dark surface. Over a white surface and the other way around and goes through it. It takes a shot at the reflection property of light. At the point when infrared light falls on a white surface, it gets reflected completely. Then again, when it falls on the dark or dim surface, it gets assimilated all things considered. The measure of reflected light will be extremely less.

4.2. Water Spraying

Soil Moisture Sensor measures the moisture level of soil and gives the dirt condition either wet or dry. On the off chance that the soil content is decreased beneath the predefined esteem it will send the flag water will begin to siphon. Generally, plant spots in order to water the plants by utilizing separation esteems from Ultrasonic Sensor. The water content in soil will be detected by the soil dampness sensors. A dirt moisture test is made up of several soil moisture sensors. A regular kind of soil moisture sensor in commercial use is a Frequency space sensor, for example, a capacitance sensor. An alternative sensor, the neutron moisture check, uses the intermediary properties of water for neutrons. Soil moisture content might be changed by means of its impact on the dielectric constant by estimating the capacitance between two cathodes embedded in the dirt. Where soil moisture prevails as free water (e.g., in sandy soils), the dielectric constant rightly corresponds to the moisture content. The test is ordinarily given a recurrence excitation to allow estimation of the dielectric constant. The readout from the test isn't straight with water content and is impacted by soil type and soil temperature. Consequently, cautious alignment is required, and long-haul security of the adjustment is faulty.

4.3. Disease detection of plants

The robot can recognize the plant leaf sicknesses by employing AI systems. One of the main tasks was to correctly identify the illness affected leaf and can discover the sort of malady by utilizing profound learning strategy in ML (Fig. 5).

The main modules included are:

- Data set: data set of plant leaves are collected which contains labelled images.
- Data resizing: images are resized which is to be given as input to the neural network.
- Training: the resized data set is used to train the neural network. The training data consist of 4000 plants which are classified as h, l, v, b.
- Testing: the testing data set contains both healthy and unhealthy leaf images. After testing images are classified as healthy or unhealthy

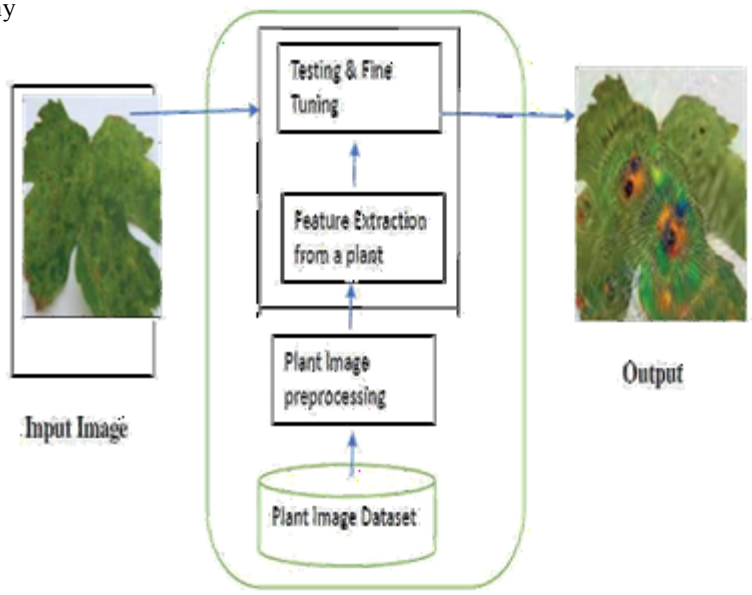

Fig. 5: Processing plant leaf

The testing generates a result either as healthy or diseased by comparing the input image with the known image data set and returns the result with a percentage of accuracy. The input data will be images of data that is the plants. There are two categories in leaf images which are healthy or unhealthy and there are four class labels: healthy(h), late-blight(l), viral(v), bacterial(b) [23].

Also, there are 4000 training images each with resolution 256x256. The input training data as well as testing data will be converted into a numpy array with input filename and its label. The label will be in the one hot encoded format. Cv2, numpy, os, tqdm libraries are imported for data resizing. The image is resized into the resolution 50*50 by using the packages in imported libraries. The training process involves creating a DNN and then passing the train data for training the network [24]. Here the tensor flow framework is used to create a neural network. The input data shape is in the form of (50,50,3), then the first layer which is the input layer to the neural network will have the same shape. There are a total of 6 hidden layers mentioned with the input size as well as the activation function that's being used. The last layer is where the fitting or converging takes place and we finally get output in that layer. It is fully connected. Here we are using two activation functions [25] 'relu' and 'softmax', 'relu' means Rectified Linear Unit [26]. This is mainly used in hidden layers in neural networks. 'softmax' is used to calculate the probability of the class labels in the output layer [27]. Dropout function is used in the fully connected layer to avoid the overfitting of the input data. Training and testing done by using 'model.fit' function. In supervised training, both the inputs and the actual outputs need to be provided. The neural network process the input and produces output. The output which is generated is compared with the desired output. If any errors in the output, it will back propagate. Feature extraction in a neural network is explained by the concept of convolution. Convolution is considered as the main building block of a CNN [28]. By Convolution we mean the mathematical mixture of two functions to produce a third function. With respect to Convolution Neural Network (CNN), the convolution is executed by the mechanism of sliding the filter or kernel over the input data. Matrix multiplication is accomplished at each location and the sum of the results are added on to the feature map. The region of our filter is also called the receptive field which is named after the neuron cells. The size of this filter is 3x3 [29].

In the testing stage, we will have a plant leaf image without label, meaning we won't know which class (h,l,v,b) the image will fall into. The already trained saved model will be loaded and then the test image will be then passed as input to the already trained model. The model based on what features it has learned will output the class which it belongs to with the help of 'model. Predict' function. By adding a new type of plant to the image data set, we can detect almost all types of diseases. we do not need external hardware devices The system will generate output with approximately 90% accuracy and the system can be fine-tuned any time for any new types of diseases, simply by adding the new disease leaf images.

4.4. Working Principle

The module is mainly divided into two. The first is a kit that performs function such as image capturing, water spraying and real time video monitoring. The second module is the diseases detection part that classifies plants based on diseases using an Artificial Neural Network. The kit moves along the black line by the black line following the algorithm and stops at each position when an obstacle is encountered which it recognizes as a plant. Fig 6 demonstrates the same.

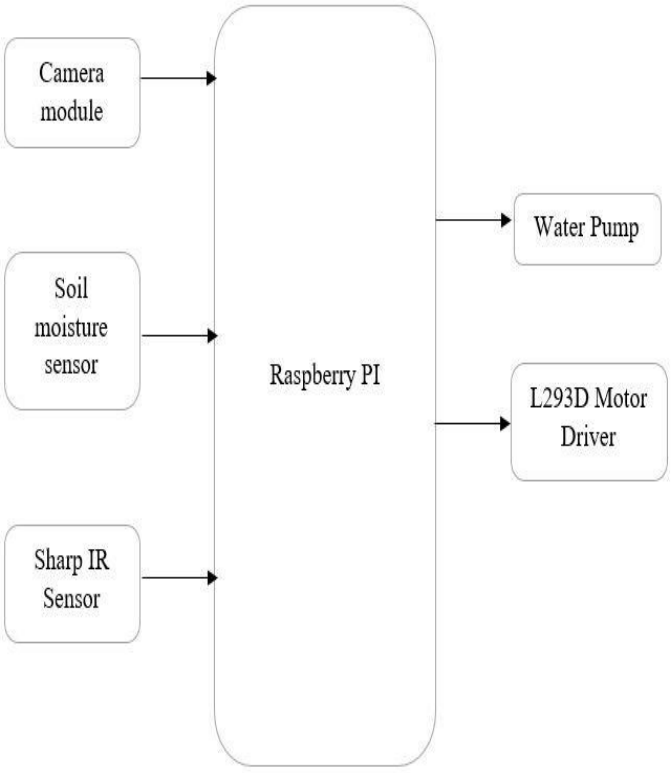

Fig. 6: Block diagram of robotic kit

The camera attached to the module captures the images and at the same time humidity of the soil is detected. On encountering the humidity value below the threshold value, water is sprayed to the plant. A real time video streaming is also provided to the user. The captured image is sent to the user's system through mail and the image is given as an input to the plant disease detection algorithm using the Convolutional Neural Network of the system which classifies the image as healthy, late blight, viral and bacterial. The heart of the system is Raspberry Pi and the corresponding function and application is done with the help of a VNC viewer. The L293D motor driver helps to convert the signals from the raspberry pi to the dc motors.

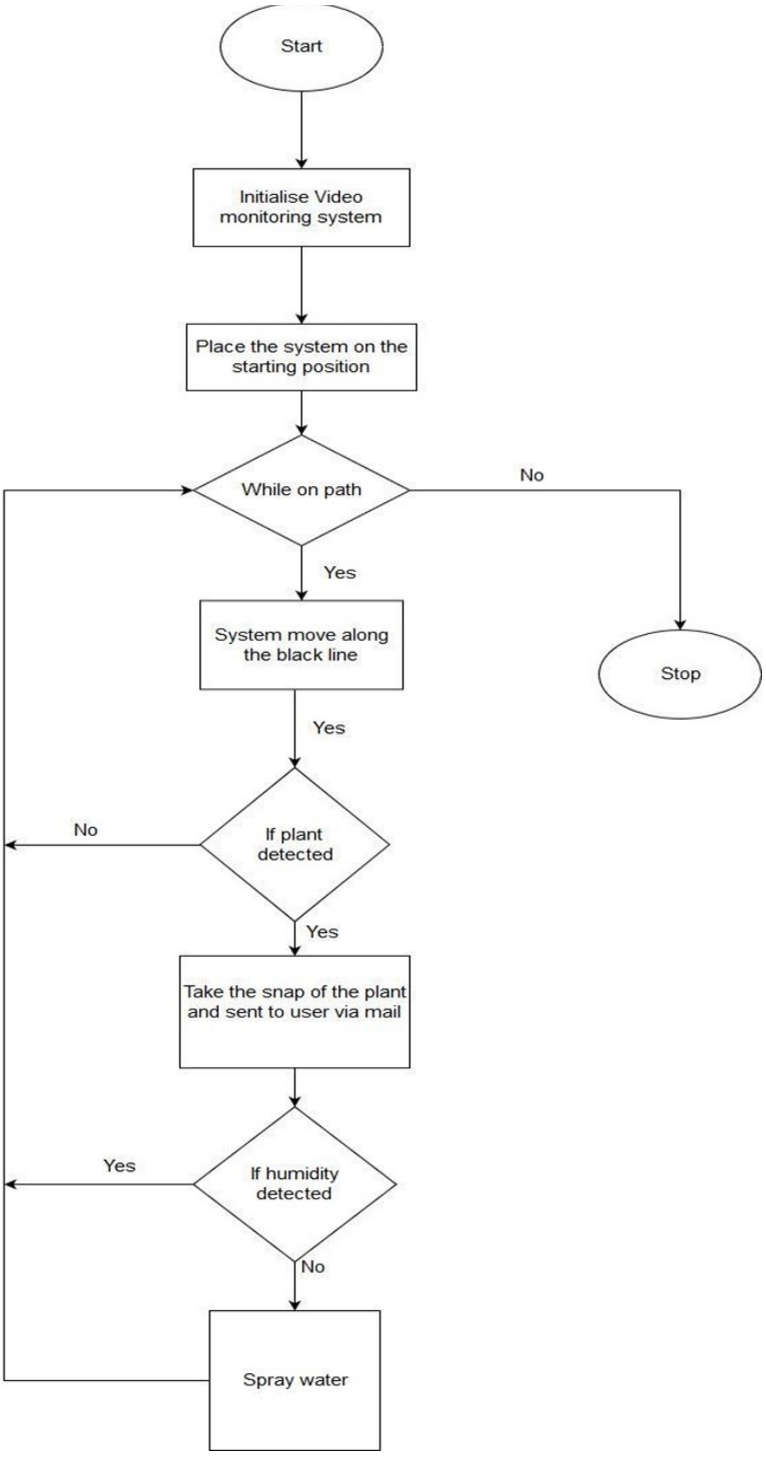

Fig 7: System Flowchart

5. Experimental Analysis

The black line following algorithm is employed in guiding the robot in the correct path. It's working is similar to that of Line following robots as depicted in Fig.8. The Line Following robot is one that identifies a black path [30]. The two IR sensors are kept in between the black line. If it detects a white line it stops. If it encounters an object it recognizes it as a plant and the image of the leaf is sent.

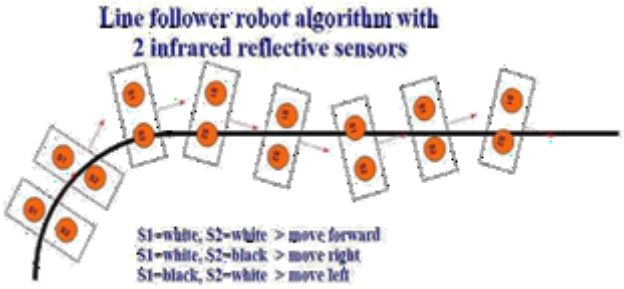

Fig. 8: Black line following adaptation

The water spraying is done uniformly for each plant as it encounters a plant. Water spraying also depends on the moisture of the soil. If there is moisture content it does not spray water. Along with this the video streaming is also done along the path till the end. Based on the leaf image captured by the system a table for the image and the corresponding result incurred for the leaf the table is depicted as shown below Table 1.

Table 1 - Captured leaf image Analysis.

Captured leaf image	Leaf name	Expected result	Experimental Result
	Tomato leaf	Late blight	late blight (correct)
	Tomato leaf	Healthy	Healthy (correct)

	Mango leaf	Healthy	Healthy (correct)
	Money plant	Late blight	Bacterial (wrong)
	Tomato leaf	Viral	Viral (correct)
	Tomato leaf	Bacterial	Bacterial (correct)

The raspberry pi console and video streaming as shown in Fig 9 and 10 respectively.

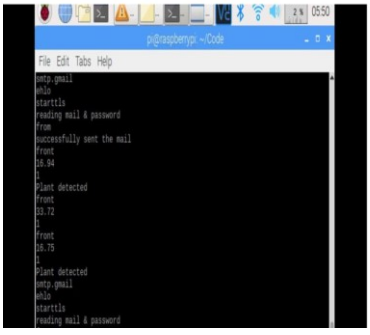

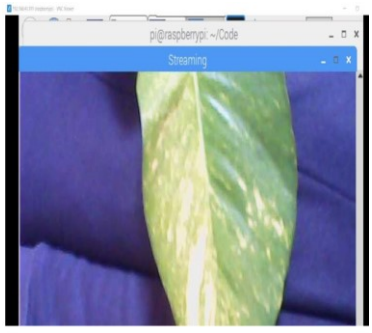

Fig 9. Raspberry Pi Console ***Fig 10. Video Streaming***

For a live plant the training was completed in 96.65 seconds and the test result was that it was bacterial.

6. Conclusion

Agriculture is one of our most important sectors for providing food, feed and fuel necessary for our existence. Autonomous kits are playing an important role in this field. In the present scenario, a wide range of such kits are available to perform different applications on various levels of agricultural process. The proposed system ROFAR concentrates mainly on disease detection and

it accurately distinguishes plants based on diseases. By inculcating new species of plants to image data set, we can detect almost all types of diseases. The system will generate an output with approximately 90% accuracy. The system can be fine-tuned any time for any new type of diseases, simply by adding the new disease leaf images. Most detection systems can detect fungal diseases only, but our system detects almost all. With this system there is no need for farmers to be present at that time and he/she could perfectly detect the diseases if it is present in the plants

7. Future Scope

We have to keep in mind that a learning curve will be present as the technologies improve in their operation capacity and sensitivity. The industrial trends appear to be moving towards large-scale efforts, so kits like this should be continuously developed. The kit designed by us, if further developed, could also do the necessary function for treatment of the detected diseases among plants. Thus, the fully autonomous kit could be developed. By making use of a gripper circuit the kit can dip the moisture sensor into each plant at each position to measure the moisture content.

REFERENCES

[1] Ji-Chun Zhao, Jun-Feng Zhang. The study and application of the IOT technology in agriculture. 2010 3rd International Conference on Computer Science and Information Technology.
[2] Pritish Sachdeva, Shrutik KatchiiḂ. A Review Paper on Raspberry Pi 2015.
[3] Thomas F. Scherer. Soil, Water and Plant Characteristics Important to Irrigation Dec. 2017.
[4] George N. Agrios. Plant Pathology, Fifth Edition 25th January 2005.
[5] S. P. Raychaudhuri, J. P. Verma, T. K. Nariani, B. Sen. The History of Plant Pathology in India Vol. 10:21-36.
[6] Nakib Hayat Chowdhury, Deloara Khushi, Md. Mamunur Rashid. Algorithm for line follower robots to follow crit ical paths with minimum number of sensors. Accepted to International Journal of Computer (IJC) 2017.
[7] J. S. Tan ; V. Teh ; H. M. Teck ; Z.H. Lim, Future farming robotic delivery system jackbot mark I, 2016 IEEE Conference on Wireless Sensors (ICWiSE).
[8] Mehran pakdaman, Mehdi Sanaatiyan, Mahdi Rezaei Ghahroudi (2010) "A Line Follower Robot from design to Implementation: Technical issues and problems" proceedings on 2010 The 2nd International Conference on Computer and Automation Engineering (ICCAE) Page(s) 5 -9.
[9] Tuan D. Le, Vignesh R. Ponnambalam, Jon G. O. Gjevestad, Pål J. From, A low- cost and efficient autonomous row- following robot for food production in polytunnels, Volume 37, Issue 2, Pages: 309-321, Journal of Field Robotics, WILEY Online library, June 2019.
[10] Jawad Iqbal, Rui Xu, Shangpeng Sun, Changying Li, Simulation of an Autonomous Mobile Robot for LiDAR-Based In-Field Phenotyping and Navigation, Robotics, 10.3390/robotics9020046, 9, 2, (46), (2020).
[11] Ege Ozgul ,Ugur Celik,.Design and implementation of semi-autonomous anti-pesticide spraying and insect repellent mobile robot for agricultural application, 5th International Conference on Electrical and Electronic Engineering (ICEEE) 2018.
[12] P. B. Sowmiya , B. K. Nagaswetha , D. Priyadharshini. Design of automatic nutrition supply system using iot technique in modern cities, 2017 International Conference on Technical Advancements in Computers and Communications (ICTACC).
[13] Sajjad Yaghoubi, Negar Ali Akbarzadeh, Autonomous robots for agricultural tasks and farm assignment and future trends in agro robots, International Journal of Mechanical & Mechatronics Engineering IJMME-IJENS Vol:13 No:03
[14] Khakal Vikas Shivaji, S. G. Galandereal. Real time video monitoring and microparameters measurement using sensor networks for efficient farming. International Conference for Convergence for Technology-2014.
[15] Jagadish Kashinath Kamble. Plant disease detector. 2018 International Conference On Advances in Communication and Computing Technology (ICACCT).
[16] Aravind, M. Daman, B. S. Kariyappa. Design and development of automatic weed detection and smart herbicide sprayer robot. 2015 IEEE Recent Advances in Intelligent Computational Systems (RAICS).
[17] Oberti R, Marchi M, Tirelli P, Calcante A, Iriti M, Tona E, et al. Selective spraying of grapevines for disease control using a modular agricultural robot. Biosyst. Eng, 2016; 146: 203–215.
[18] Gonzalez-de-Soto M, Emmi L, Perez-Ruiz M, Aguera J, Gonzalez-de-Santos P. Autonomous systems for precise spraying – Evaluation of a robotised patch sprayer. Biosyst. Eng., 2016; 146: 165–182.
[19] Adamides G, Katsanos C, Parmet Y, Christou G, Xenos M, Hadzilacos T, et al. HRI usability evaluation of interaction modes for a teleoperated agricultural robotic sprayer. Appl. Ergon. 2017; 62: 237–246.
[20] Tanha Talaviya, Dhara Shah, Nivedita Patel, Hiteshri Yagnik, Manan Shah, Implementation of artificial intelligence in agriculture for optimisation of irrigation and application of pesticides and herbicides, Artificial Intelligence in Agriculture, Volume 4, 2020, Pages 58-73, ScienceDirect, https://doi.org/10.1016/j.aiia.2020.04.002. (http://www.sciencedirect.com/science/article/pii/S258972172030012X).
[21] Midtiby H S, Mathiassen S K, Andersson K J, Jørgensen R N. Performance evaluation of a crop/weed discriminating microsprayer. Comput. Electron. Agric., 2011; 77(1): 35–40.

[22] Choudhury D. Roy. Networks and Systems Paperback Jun 2013.
[23] Noa Schor, Avital Bechar. Robotic Disease Detection in Greenhouses: Combined Detection of Powdery Mildew and T omato Spotted Wilt Virus. IEEE ROBOTICS AND AUTOMATION LETTERS. PREPRINT VERSION. ACCEPTED December, 2015.
[24] Schmidhuber. Deep learning in neural networks: An Overview of Neural networks. vol. 61, pp. 85–117, 2015.
[25] Chigozie Enyinna Nwankpa, Winifred Ijomah. Activation Functions: Comparison of Trends in Practice and Research for Deep Learning. arXiv:1811.03378v1 [cs.LG] 8 Nov 2018.
[26] Charu C. Aggarwal. Neural Networks and Deep Learning: A Textbook 25 August 2018.
[27] Christopher Bishop. Neural networks for pattern recognition, 23 Nov 1995.
[28] Muluken Hailesellasie, Syed Rafay Hasan. FPGA-Based Convolutional Neural Network Architecture with Reduced Parameter Requirements 2018 IEEE International Symposium on Circuits and Systems (ISCAS).
[29] Alex Krizhevsky, Ilya Sutskever. ImageNet Classification with Deep Convolutional Neural Networks. Advances in neural information processing systems January 2012.
[30] Juing-Huei Su, Chyi-Shyong Lee. An intelligent line-following robot project for introductory robot courses. World T ransactions on Engineering and T echnology Education Vol.8, No.4, 2010.

Back

RESEARCH-ARTICLE

DIO messages and trickle timer analysis of RPL routing protocol for UAV-assisted data collection in IoT

Authors: Bishmita Hazarika, Rakesh Matam, Mithun Mukherjee, Varun G Menon Authors Info & Claims

DroneCom '20: Proceedings of the 2nd ACM MobiCom Workshop on Drone Assisted Wireless Communications for 5G and Beyond
• September 2020 • Pages 86–90 • https://doi.org/10.1145/3414045.3415944

Published: 07 October 2020 Publication History Check for updates

ABSTRACT

Routing protocol for low-power and lossy networks (RPL) is an widely-used IPv6 routing protocol for lossy wireless networks with the power constrained devices in Internet of Things (IoT). It is a proactive protocol that constructs a destination oriented directed acyclic graph (DODAG) rooted at the single destination called the root node that resides at unmanned aerial vehicle (UAV). Specifically, a DODAG

messages incur additional energy consumption, RPL uses the Trickle algorithm to dynamically adjust the transmission windows. In this paper, we analyze the effect of the two parameters, namely, DIO-

Back

selection of these parameters saves a significant amount of energy with different parameter settings in UAV-assisted IoT networks.

References

1. Hazrat Ali. 2012. A performance evaluation of rpl in contiki.

2. Cosmin Cobarzan, Julien Montavont, and Thomas Noel. 2014. Analysis and performance evaluation of RPL under mobility. In *2014 IEEE symposium on computers and communications (ISCC).* IEEE, 1--6.

3. Badis Djamaa and Mark Richardson. 2015. Optimizing the trickle algorithm. *IEEE Communications Letters* 19, 5 (2015), 819--822.

Show All References

Cited By

View all

Nayak S and Ghosh S. (2023). RPL Routing Protocol for Data Transmisison in Internet of Things Applications 2023 2nd International Conference for Innovation in Technology (INOCON). 10.1109/INOCON57975.2023.10101305. 979-8-3503-2092-3. (1-8).

https://ieeexplore.ieee.org/document/10101305/

Index Terms

DIO messages and trickle timer analysis of RPL routing protocol for UAV-assisted data collection in IoT

Computer systems organization

Back

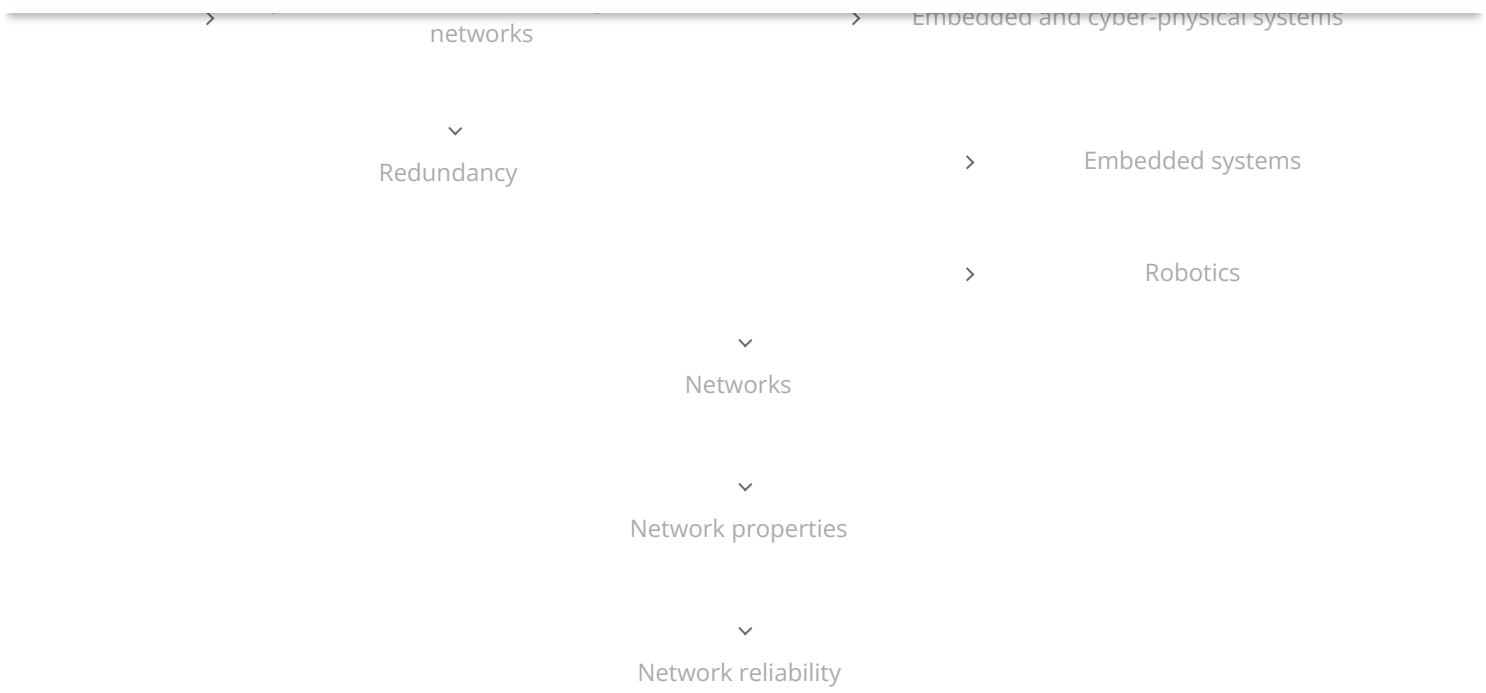

Recommendations

Mobility Aware RPL (MARPL): Mobility to RPL on Neighbor Variability

Green, Pervasive, and Cloud Computing

Read More

Probability Based Improved Broadcasting for AODV Routing Protocol

CICN '11: Proceedings of the 2011 International Conference on Computational Intelligence and Communication Networks

Read More

Design and implementation of a mobility support adaptive trickle algorithm for RPL in vehicular IoT networks

Read More

Comments

Back

Comments should be relevant to the contents of this article, (sign in required).

Got it

0 Comments

Share **Best** **Newest** **Oldest**

Nothing in this discussion yet.

Privacy **Do Not Sell My Data**

View Table Of Contents

‹ Back

Detection of Recoloring and Copy-Move Forgery in Digital Images

Jijina M.T ; Litty Koshy ; Gayathry.S. Warrier All Authors

Abstract: Due to the availability of numerous image manipulation tools, fraud images can be generated very easily and effectively. These fraud images are quite difficult to recogni... **View more**

Metadata

Abstract:
Due to the availability of numerous image manipulation tools, fraud images can be generated very easily and effectively. These fraud images are quite difficult to recognize. A section of the image is copied and pasted at some other location on the same image in copy-move forgery to drop meaningful objects or to bring additional information which is not present actually in the image. Whereas, the image recoloring techniques normally change the images via a variety of mechanisms like contrast enhancement and colorization. In the proposed method, copy move forgery detection is based on similarities in the images and finding the forged part by using threshold and contouring techniques. Recolored image detection uses a convolution neural network with three layers which outputs the probability of recoloring. As the techniques for image forging are developing faster, the necessity of highly efficient and accurate image forgery detection also increases. Here, this proposed system focuses on both recoloring and copy-move forgery detection.

Published in: 2020 Fifth International Conference on Research in Computational Intelligence and Communication Networks (ICRCICN)

Date of Conference: 26-27 November 2020 **INSPEC Accession Number:** 20301118

Date Added to IEEE *Xplore*: 21 December 2020

DOI: 10.1109/ICRCICN50933.2020.9296173

ISBN Information:

Publisher: IEEE

Conference Location: Bangalore, India

Contents

Numerous digital images are generated by different devices nowadays. These images are spread by various newspapers, television channels, and different media. Various legal and scientific businesses use digital images as confirmation of certain situations and are used to make crucial decisions. Forgery in images can be defined as the manipulation of images to hide some useful information about the image. Different types of software tools, like Photoshop, are applied to make forged images, and these forged images look like real images by human vision. Unluckily, there are a lot of inexpensive and high-resolution digital cameras and advanced photo editing software available nowadays, hence it is very easy to produce fraud images and the discovery of these manipulated images is much challenging through human eyesight since they may not be leaving any visual clues that indicate the image forgery. These facts challenge the authenticity of digital images/photographs. Therefore, image forensic techniques for forged images discovery are crucial.

Published: 2012

Show More

Morphological Operators on Hypergraphs for Colour Image Processing

V Bino Sebastian ; Nuja M Unnikrishnan ; Neenu Sebastian ; Rosebell Paul All Authors

Abstract: This article is an extension of morphological operators on hypergraphs to work with colour images. Morphological operators on hypergraphs are useful for binary and graysc... **View more**

Metadata

Abstract:
This article is an extension of morphological operators on hypergraphs to work with colour images. Morphological operators on hypergraphs are useful for binary and grayscale image processing. The preliminary experimental results related to the extension of these operators to colour images is presented in this paper. The results on colour images are promising and is a better alternative for the existing methods.

Published in: 2020 Advanced Computing and Communication Technologies for High Performance Applications (ACCTHPA)

Date of Conference: 02-04 July 2020

INSPEC Accession Number: 20033605

Date Added to IEEE *Xplore*: 06 October 2020

DOI: 10.1109/ACCTHPA49271.2020.9213191

ISBN Information:

Publisher: IEEE

Conference Location: Cochin, India

Contents

I. Introduction

Mathematical morphology is the first consistent non-linear image analysis theory. Originally it was defined on a set theoretic framework and used for processing binary images and extended to grayscale images. Despite its continuous origin, it was soon recognised that the roots of the theory were in algebraic theory, notably the framework of complete lattices. This allows the theory to be completely adaptable to non-continuous spaces, such as graphs [4] , hypergraphs [3] and simplicial complexes [5] . Extending Mathematical Morphology to colour images is an active area of research in image processing [8 , 18 , 9] . There is no natural extension of the morphological operators to colour images. This is because colour images does not admit a partial ordering [11] . Image denoising is one of the most important operations in image processing. Salt and pepper noise is very common in image processing applications and noise reduction is a very active area of research in this field [12] . Morphological filtering is one of the most reliable techniques for salt and pepper noise reduction [2 , 4 , 5] . Our objective is to utilise the morphological operators defined on hypergraphs to remove this noise from colour iamges [2 , 16] .

Authors

Figures

References

Keywords

Metrics

Copy-Move Forgery Detection and Performance Analysis of Feature Detectors

Publisher: IEEE

Litty Koshy ; S. PraylaShyry **All Authors**

Abstract: Now a days, the digital image integrity are remarkably important for the exchange of data which are generally utilized for different applications like fraud detection, th... **View more**

Metadata

Abstract:

Now a days, the digital image integrity are remarkably important for the exchange of data which are generally utilized for different applications like fraud detection, therapeutic imaging, reporting, and advanced crime investigation. Digital images can easily be forged with the advancement of image manipulation tools and information technology. The commonly used image forgery technique in digital forensic filed is Copy-move forgery. The two fundamental classifications for identifying copy-move forged images are keypoint-based and block- based method. Block-based strategies have the burden of high computational expense because of the enormous number of image blocks and it fails to deal with different geometric transformations. On the contrary, keypoint-based methodologies can overwhelmed these two draw-backs however are discovered hard to manage smooth locales. As a result, these two methodologies are combined and proposed a effective copy-move forgery detection. Also, we accomplish a comparative study between different keypoint detectors and feature matching algorithms used to determine computational complexity of each.

Published in: 2020 International Conference on Communication and Signal Processing (ICCSP)

Date of Conference: 28-30 July 2020 **INSPEC Accession Number:** 19914092

Date Added to IEEE *Xplore*: 01 September 2020

DOI: 10.1109/ICCSP48568.2020.9182066

ISBN Information:

Publisher: IEEE

Conference Location: Chennai, India

Contents

W ITH the development of computer technology duplication related to images have increased exponentially. In past few decades more and more researches have been undergoing to detect and rectify tampered images. Copy-move forgery is one of the most popular image forgery techniques in which a region of an image is copied and pasted into another region of the same image. Since the copied region is from same image thus it may have same color characternoise component etc. There have been various techniques which are prevalent for matched keypoints –3] but are ineffective for forgery detection very well. To achieve both the requirements with moderately high accuracy we implement a segmentation method and feature point matching.

Authors

Figures

References

Citations

Keywords

Metrics

More Like This

Robust Affine Invariant Feature Extraction for Image Matching
IEEE Geoscience and Remote Sensing Letters
Published: 2008

Feature Extraction and Image Matching of 3D Lung Cancer Cell Image
2009 International Conference of Soft Computing and Pattern Recognition
Published: 2009

Show More